ABSTRACT

Title of Thesis: ACTIVE CONTROL OF NON-RECIPROCAL ACOUSTIC METAMATERIAL WITH A DYNAMIC CONTROLLER

Suraj Raval
Master of Science, 2019

Thesis directed by: Professor Amr Baz
Department of Mechanical Engineering

Reciprocity is one of the fundamental properties in the field of wave propagation. In acoustics, this property helps in various practical applications. But, breaking this reciprocity also has useful applications. As a result of which, many researchers have tried to break the reciprocity in acoustics, which is comparatively difficult, unlike in fields such as electro-magnetics.

Majority of these proposed methods to break the reciprocity are hard-wired systems, which work for a very limited frequency range. Thus, we have introduced a non-reciprocal metamaterial having boundary control with the help of piezoelectric sensors and actuators. A theoretical model is introduced to induce the non-reciprocal behavior, and it is backed up by providing experimental evidence.

Our setup consists of a cylindrical cell made up of acrylic, filled with water, having four piezo sensors/actuators, two on each end. The idea is to excite the piezo cell through an actuator on one side, collect the resulting signal from the piezo sensor on the other side, and perform appropriate mathematical operations

on this signal to produce a feedback/control signal via a specially designed dynamic control action. This control signal affects the propagation of pressure waves through the water medium inside the cell as it introduces a virtual gyroscopic effect of controlled magnitude and direction. Thus, this is how non-reciprocity is introduced and controlled into the metamaterial cell. The obtained theoretical and experimental results demonstrate the effectiveness of the dynamic controller in breaking the acoustic reciprocity. Extension of this work to multi-cell metamaterial configuration is natural extension to be pursued.

ACTIVE CONTROL OF NON-RECIPROCAL ACOUSTIC METAMATERIAL WITH A DYNAMIC CONTROLLER

by

Suraj Raval

Thesis submitted to the Faculty of the Graduate School of the
University of Maryland, College Park in partial fulfillment
of the requirements for the degree of
Master of Science
2019

Advisory Committee:
Dr. Amr Baz, Advisor
Dr. Balakumar Balachandran
Dr. Nikhil Chopra

Acknowledgments

I owe my gratitude to all the people who have made this thesis possible and because of whom my graduate experience has been one that I will cherish forever.

First and foremost I'd like to thank my advisor, Professor Amr Baz for giving me an invaluable opportunity to work on challenging and extremely interesting projects over the past year or so. He has always made himself available for help and advice and there has never been an occasion when I've knocked on his door and he hasn't given me time. It has been a pleasure to work with and learn from such an extraordinary individual, who is an expert in the field of vibrations, acoustics and control.

Thanks are due to Professor Balakumar Balachandran and Professor Nikhil Chopra for agreeing to serve on my thesis committee and for sparing their invaluable time reviewing the manuscript.

Table of Contents

List of Figures

List of Abbreviations

AAMM	Active Acoustic Metamaterial
ANAM	Active Non-reciprocal Acoustic Metamaterial
DAQ	Data Acquisition Device
APDL	*ANSYS* Parametric Design Language
TSMM	Temporal and Spatial Modulation Method

Chapter 1: Introduction

1.1 Concept of Reciprocity

Given that the medium of propagation is stationary, reciprocity is a fundamental property, which applies to waves travelling in that medium. Thus, if waves travel from point A to point B, then the wave travels in the same way from point B to point A and that symmetry is called as *"reciprocity"*. Thus, we can say that the direction of travel doesn't affect the waves as long as the points in the medium are fixed. Now, this property is actually very beneficial, resulting in applications such as ease of measurements. For example, in cases where we need to measure the noise in submarines, engines, etc., the change in the position of speaker and microphones wouldn't affect the results and would make the measurements more convenient, due to reciprocity. In most of these applications, reciprocity generally solves the problem of space constraints and budget constraints. Generally, microphones occupy much lesser space compared to the loudspeakers, so it is more convenient to use microphones in hard-to-reach regions. Secondly, loudspeakers are generally more expensive compared to the microphones. But due to the reciprocity theorem, we can get away with using an array of microphones instead of a loudspeaker.

Reciprocity, as a concept was first introduced in a paper by Hermann von Hel-

moltz, in 1860. The paper showed the exhibition of reciprocity inside open-ended pipes. However, a more comprehensive understanding of the concept of reciprocity was introduced by Lord Rayleigh in 1873. He showed that, when the application of harmonic force at a given point A generates an oscillatory displacement at point B, the complex ratio of this oscillatory displacement to the harmonic force remains constant, even when we interchange the position of points A and B. Rayleigh's theory is applied to linear and elastic systems, which have physical parameters which are time-invariant in nature. Air at rest, satisfies these criteria as a medium of propagation. The input parameter in the air medium is actually air's rate of change of displacement, which produces the sound waves and is known as the velocity *'V'*. And, the output parameter is the force *'F'* applied by this air waves on the transducer. Thus, Rayleigh talks about the application of reciprocity to this ratio *'F/V'*. The figure below tries to simplify this concept for any given acoustic medium. If at a given point A, the acoustic waves are excited, then the sound pressure produced at a given B, due to this excitation, is same in magnitude and phase to the one produced, on interchanging the points A and B.

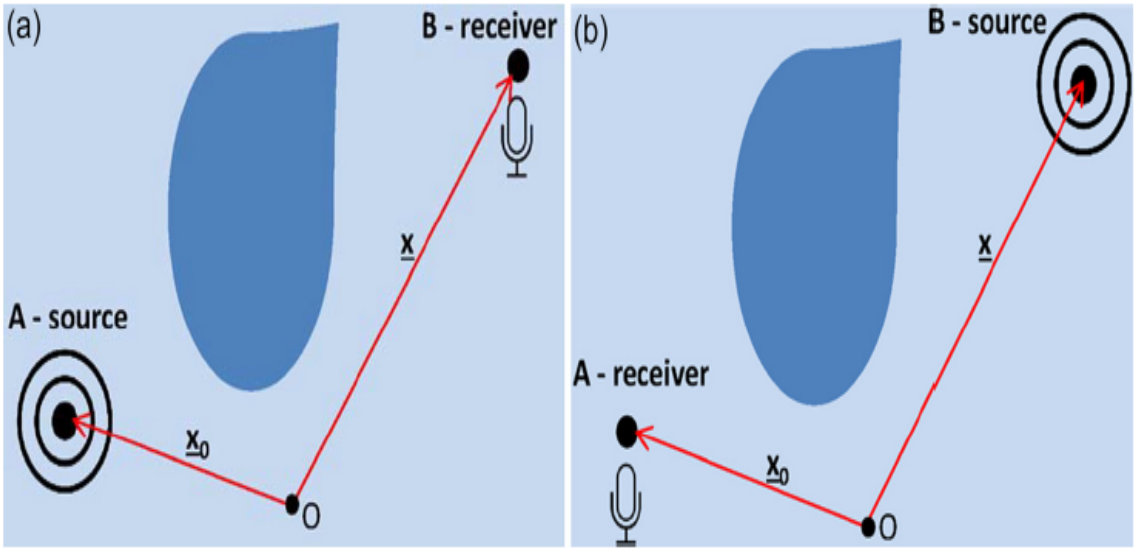

Figure 1.1: Depiction of Reciprocity in an acoustic medium (Samarasinghe and Abhayapala, 2017)

The Rayleigh's principle can be extended to a system which has single input and multiple outputs too. For example, if there are *'S'* locations in an acoustic medium, which act as sources. And, there are *'R'* locations in the acoustic medium which acts as receivers. Then, the Rayleigh's reciprocity principle is applicable to every pair of source and receiver.

1.2 Reciprocity with respect to the Green's function

The Green's function satisfies the inhomogeneous wave equation. Thus, The Green's function is a solution to the inhomogeneous wave equation. In the figure shown above, with respect to the origin *'O'*, the point *'x'* denotes the receiver location and the point 'x_0' denotes the source position. Thus, using the Green's function, we can display the reciprocity between the points 'x' and 'x_0' as :

$$G(x|x_0, k) = G(x_0|x, k) \tag{1.1}$$

Where, *'k'* denotes the wavenumber.

1.3 Mathematical Representation

On considering a 2-D space co-ordinate system, it is assumed that the variables of the medium are functions of two spatial variables, namely x_1 and x_3. As a result of this assumption, the wave equations of the acoustic waves are reduced to scalar wave equations from the corresponding vector wave equations. The Fourier transform of a real function is given as :

$$U(\omega) = \int_{-\infty}^{\infty} exp(-j\omega t)u(t)dt \tag{1.2}$$

The inverse of the above equation can be written as :

$$U(t) = (1/\pi)Re \int_{-\infty}^{\infty} exp(j\omega t)\chi(\omega)U(\omega)d\omega \tag{1.3}$$

Where,

$$\chi(\omega) = \begin{cases} 0 & \omega < 0 \\ 1/2 & \omega = 0 \\ 1 & \omega > 0 \end{cases} \tag{1.4}$$

Now, in the frequency domain, the general form of the 2-D equations is given

as :

$$j\omega\alpha P + \partial_i Q_i = B \tag{1.5}$$

And,

$$j\omega\beta Q_i + \partial_i P = C_i \tag{1.6}$$

In the above equations, i takes the values of 1 and 3. Now, eliminating Q_i from the above two equations, gives the following scalar equation for waves in 2-D :

$$\beta\partial_i((1/\beta)\partial_i P) + \alpha\beta\omega^2 P = \beta\partial_i((1/\beta)C_i) - j\omega\beta B \tag{1.7}$$

In the above equations, P,Q_1 and Q_3 stand for the wave-field. They are functions of x(x_1,x_3) and ω. While, B,C_1 and C_3 are the sources as functions of x(x_1,x_3) and ω. α and β are the parameters of the acoustic medium. They are also functions of x(x_1,x_3) and ω.

Now, for the acoustic medium, the variables in the above equations can be replaced as shown below :

P = -T (Stress), $Q_i = V_i$ (Particle Velocity), α = k (Compressibility), $\beta = \rho$ (Mass Density), $C_i = F_i$ (Force Density).

Now, it is assumed that x_3 is the direction of wave propagation along the axis. Thus, x_1 gives the lateral co-ordinate. While, x_3 gives the axial co-ordinate. The medium bounds in both the directions can be seen in the figure below. The figure depicts the configuration for which the reciprocity theorem is to be derived. P^+ and

P^- are the one way fields and are coupled.

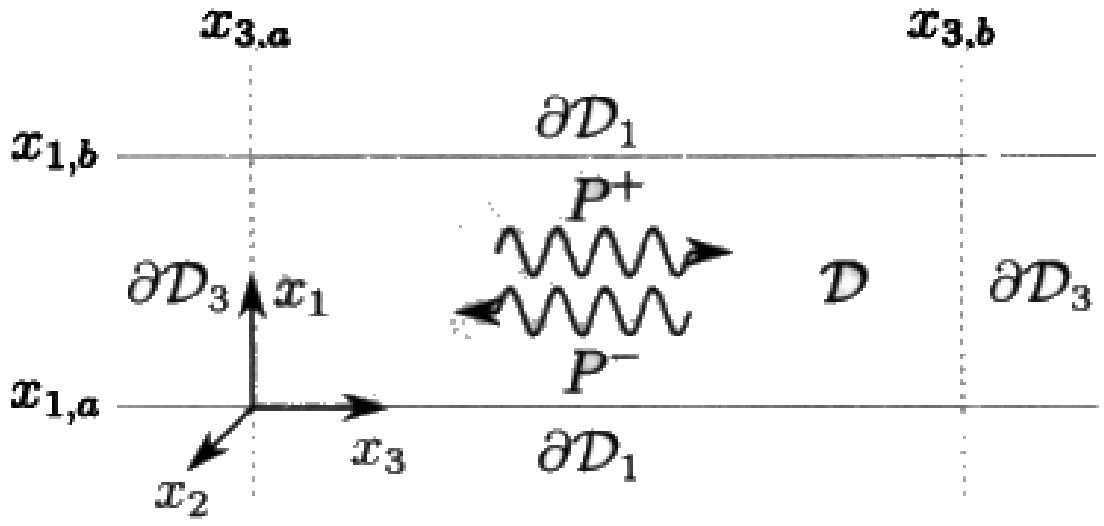

Figure 1.2: configuration to derive the reciprocity theorem (Wapenaar *et al.*, 2001)

By eliminating Q_1 from the equations 1.5 and 1.6, we can get the the equations shown below. This equation takes into consideration the preferred direction.

$$\partial_3 Q = \hat{A} Q + D \tag{1.8}$$

Where, Q is the wave-field vector, which is given as :

$$Q = \begin{pmatrix} P \\ \\ Q_3 \end{pmatrix} \tag{1.9}$$

Also, D is the vector relating to the source, which is given as :

$$D = \Big(B - (1/j\omega)\partial_1 (C_1/\beta) \Big) \tag{1.10}$$

And, $\hat{A}$ is the operator matrix, which is given as :

$$\hat{A} = \begin{pmatrix} 0 & -j\omega\beta \\ -j\omega(\alpha + (1/\omega^2)\partial_1(\partial_1/\beta)) & 0 \end{pmatrix} \tag{1.11}$$

1.4 Unidirectional wave equation

The square root operator, which will be introduced in this section, is critical for the one way wave equation. This operator plays an important role in the diagonalization of the operator matrix $\hat{A}$. Thus, the diagonalized form of this operator matrix $\hat{A}$ is used to extract the one-way wave equation from the wave field vector Q. Now, the matrix $\hat{A}$, which has been mentioned previously, can be rewritten as :

$$\hat{A} = \begin{pmatrix} 0 & -j\omega\beta \\ (1/j\omega\beta^{1/2})(H_2\beta^{-1/2}) & 0 \end{pmatrix} \tag{1.12}$$

Where, H_2 is the square root operator and H_1 is the square root of the square root operator. Further, we can write the operator matrix as :

$$\hat{A} = \hat{L}\hat{H}\hat{L^{-1}} \tag{1.13}$$

Where, $\hat{H}$ is an operator matrix which is diagonal in nature :

$$\hat{H} = \begin{pmatrix} -jH_1 & 0 \\ 0 & jH_1 \end{pmatrix} \tag{1.14}$$

And,

$$\hat{L} = \begin{pmatrix} \hat{L_1} & \hat{L_1} \\ \hat{L_2} & -\hat{L_2} \end{pmatrix} \tag{1.15}$$

Where,

$$\hat{L_1} = (\omega\beta/2H_1)^{1/2} \tag{1.16}$$

$$\hat{L_2} = (H_1/2\omega\beta)^{1/2} \tag{1.17}$$

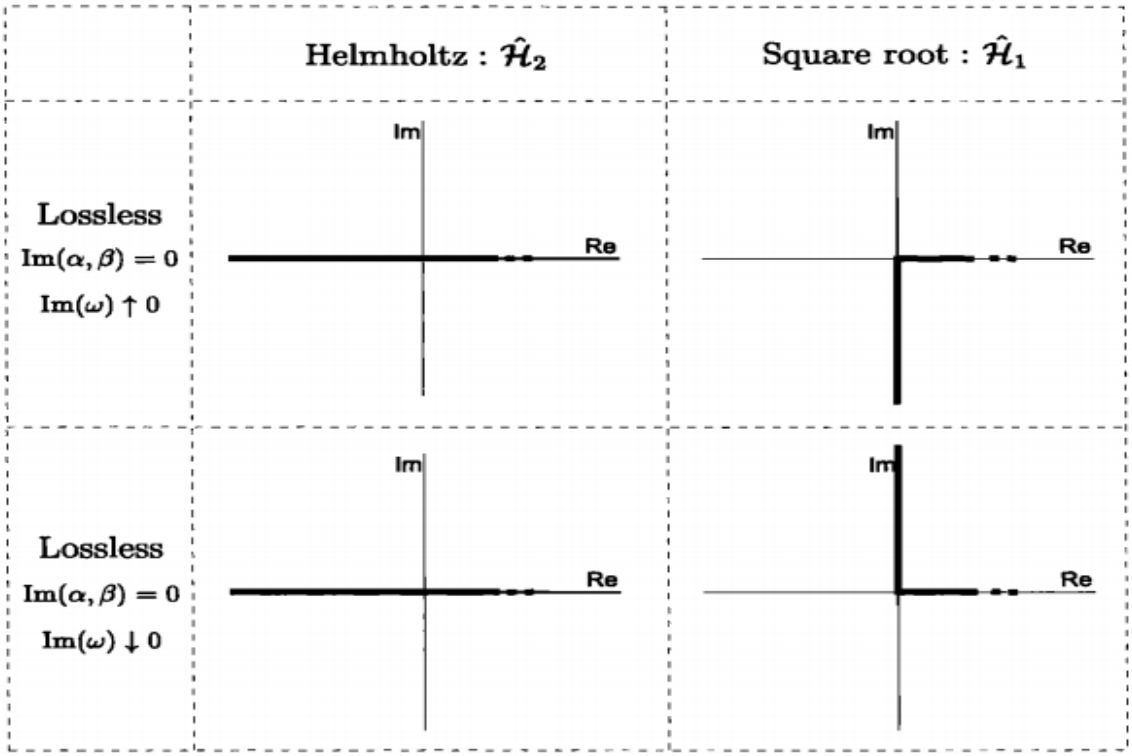

Figure 1.3: Eigenvalue spectrum for the Helmoltz and the square-root operator (Wapenaar *et al.*, 2001)

The above figure shows the eigenvalue spectrum of various operators in a complex plane for a lossless medium. A new unidirectional wave field vector P is

introduced such that :

$$P = \begin{pmatrix} P^+ \\ \\ P^- \end{pmatrix} \tag{1.18}$$

Here, P^+ and P^- are unidirectional wave fields. P^+ propagates in the positive x_3 direction, while P^- propagates in the negative x_3 direction. Now, substituting the equation (1.13) into equation (1.8), we get :

$$\hat{L^{-1}}\partial_3 Q = \hat{H}\hat{L^{-1}}Q + \hat{L^{-1}}D \tag{1.19}$$

The above equation implies that P is defined in such a way that :

$$Q = \hat{L}P \tag{1.20}$$

This leads to the unidirectional wave equation :

$$\partial_3 P = \hat{B}P + S \tag{1.21}$$

Where, $\hat{B}$ is the unidirectional operator matrix, which is written as :

$$\hat{B} = \hat{H} - L^{-1}\partial_3\hat{L} \tag{1.22}$$

Now, the unidirectional source S is defined in such a way that :

$$D = \hat{L}S \tag{1.23}$$

Here,

$$S = \begin{pmatrix} S^+ \\ \\ S^- \end{pmatrix} \tag{1.24}$$

S^+ and S^- correspond to the source for the unidirectional fields P^+ and P^- respectively. The matrix $\hat{B}$ is written as :

$$\hat{B} = \begin{pmatrix} -jH_1 & 0 \\ \\ 0 & jH_1 \end{pmatrix} + \begin{pmatrix} \hat{T} & -\hat{R} \\ \\ -\hat{R} & \hat{T} \end{pmatrix} \tag{1.25}$$

Where, $\hat{T}$ is a transmission operator, given as :

$$\hat{T} = -(\hat{L_1^{-1}}\partial_3\hat{L_1} + \hat{L_2^{-1}}\partial_3\hat{L_2})/2 \tag{1.26}$$

And, $\hat{R}$ is the reflection operator, which is given as :

$$\hat{R} = -(\hat{L_1^{-1}}\partial_3\hat{L_1} - \hat{L_2^{-1}}\partial_3\hat{L_2})/2 \tag{1.27}$$

Thus, we can see that the unidirectional operator matrix $\hat{B}$ is different from $\hat{A}$, because it clearly differentiates the flow (propagation) and the scattering.

1.5 Source of Non-Reciprocity in Acoustics

Reciprocity refers to the value of pressure being measured at a certain point with a source at a different point, being the same as, when the points are interchanged and the pressure is measured at the other point. Thus, reciprocity makes the acoustic system independent of direction. Reciprocity can be referred to as

one of the fundamental properties of the wave equation in a given linear medium. External magnetic field is generally used for breaking of reciprocity in an electromagnetic medium, but it is much more simpler compared to breaking of reciprocity in an acoustic medium. Breaking this reciprocity has tremendous applications in the field of acoustics, energy harvesting, noise control, transducer technology, etc. This non-reciprocity can result in acoustic insulation, which is very helpful in the field of medical technology with equipment such as ultrasonic sensors as well as other imaging technologies. As a result of which, many different approaches have been tried in order to break the reciprocity. Since the electrical diode has come into practice, people have been trying to create diodes with other forms of energy, such as the acoustic energy.

Many different methods have been used to introduce non-reciprocity. Jung-San Chen *et al.*, (2016) used alternate layers of water and metamterial with complex mass density. While, E. Walker *et al.*, (2018) conducted experiments to prove that breaking the PT symmetry results in the introduction of non-reciprocity in acoustics. Dai and Zhu (2013) proposed a new class of metamaterials for the introduction of nonreciprocity in acoustics. They used temporal modulation of phase velocity inside active acoustic metamaterials to achieve nonreciprocity. Using a combination of material damping and the effect of coriolis acceleration in a flexible rotating ring, Beli *et al.*, (2018) showed that it results in breaking of the time-reversal symmetry. Karkar and Collet (2017) proposed a semi-active acoustic device which introduces nonreciprocity using the concept of programmable boundary conditions.

Over the past decade, it has been demonstrated that a promising and a more

effective acoustic system can be built with the help of metamaterials. Due to the unusual dynamic properties that the metamaterials exhibit, they work very well in order to filter out low frequency acoustic waves. Another such popular approach is the introduction of periodicity in material arrangement which generally uses impedance mismatch to control the propogation of acoustic waves through a medium. Chen *et al.*, (2016) proposed an asymmetric transmission device. The device is based on a one-dimensional layered structure with gradient thickness. The system is constituted by water and by a metamaterial with a complex mass density. They have proposed a numerical model of the asymmetric transmission, as well as a finite element model to see the effect of the gradient thickness on the acoustic wave rectification. Chen *et al.*, (2016) proposed the one-dimensional layered structure as shown in Figure (1.4).

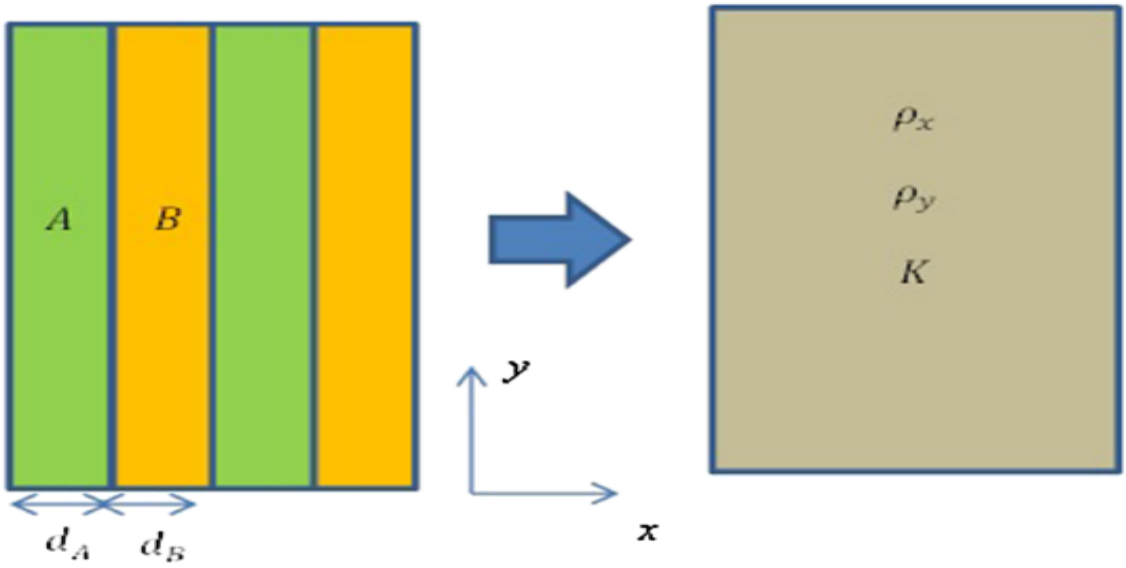

Figure 1.4: 1-D Layered structure and it's equivalent structure (Chen *et al.*, 2016)

There are layers of two different alternating materials. the whole setup being placed inside a water medium. Numerical simulations have been carried out for three

different scenarios. They are : the thickness of the layer is same, increasing as an arithmetic progression, increasing as a geometric progression. Thus, the asymmetric transmission is introduced when the incident wave is travelling from the other side in cases two and three. The numerical and the finite element simulation results can be seen in the images. The finding of an optimum thickness gradient for this layered structure should increase the asymmetry in the system.

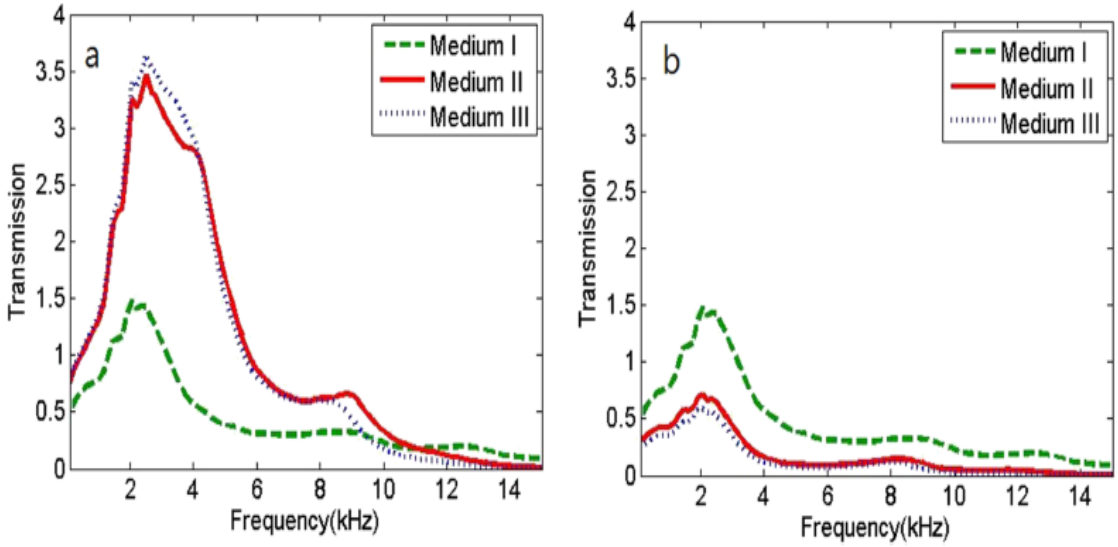

Figure 1.5: Variation of transmission with frequency, with waves emitted from, (a) left side of the layered structure, (b) right side of the layered structure (Chen *et al.*, 2016)

Walker *et al.*, (2018) proposed a setup, wherein, a phononic crystal, submerged in water and comprising of asymmetric rods that breaks the T symmetry. The viscosity of water is an important factor in doing so.

Dai and Zhu (2013) tries to solve the problem of introducing nonreciprocity into acoustics by introducing active acoustic metamaterials with dynamically modulated phase velocity. The method proposed is "gauge-potential based" one way

mode conversion, in order to introduce nonreciprocity. The findings show that a phononic transition (in a time-varying medium) with a shift in frequency can be allowed to happen in propagating forward, due to the phenomenon of constructive interference. But, this shift is not allowed in the backward propagation due to the occurrence of destructive interference. This results in a Doppler shift which is unidirectional in nature.

Beli *et al.*, (2018) have proposed the use of a flexible rotating elastic ring to induce nonreciprocal behavior, which is used in construction of a mechanical circulator having three ports. The equations of motion of the flexible rotating ring were described by the Eulerian reference frame.

Now, Karkar *et al.*, (2017) proposed an acoustic isolator model which is shown in the figure.

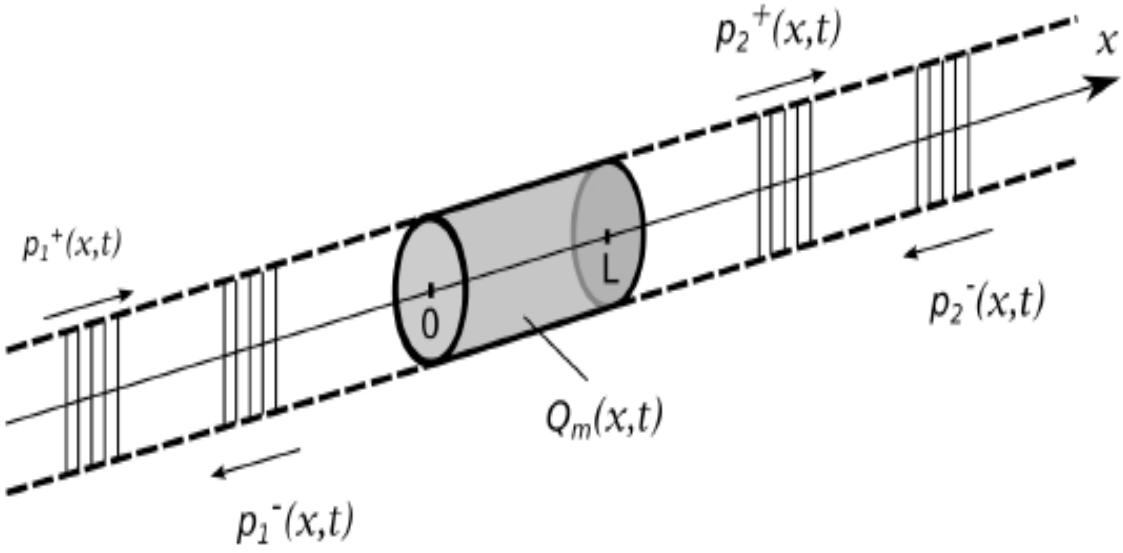

Figure 1.6: Acoustic Isolator (1D) (Karkar *et al.*, 2017)

As seen in the figure above, when an incident wave p_1^+, hits the left side of

the isolator, it passes through the isolator, without any reflection and absorption. It comes out from the other side as the wave p_2^+. Now, when the wave p_2^- from the other side is incident on the isolator, a part of the wave (p_2^+) is reflected, a part is absorbed and a part (p_1^-) is transmitted through. Thus, this isolator basically acts as a diode as it allows transmission in only one direction. These acoustic diodes have critical applications in the industry. For example, in an aeroplane, the noise from the engine situated in the wings, shouldn't be able to travel inside the fuselage, while, on the other hand, the noise generated inside the fuselage (by the passengers), should be thrown out. Thus, it is an example where unidirectional transmission noise is necessary.

The S matrix is a matrix which links the input and the output of the system. This system has two inputs and two outputs. p_1^+ and p_2^- are the input waves, while the other two are the output waves. Thus, the equation is written as :

$$\begin{bmatrix} p_1^- \\ p_2^+ \end{bmatrix} = S \begin{bmatrix} p_1^+ \\ p_2^- \end{bmatrix} \tag{1.28}$$

Where,

$$S = \begin{bmatrix} S11 & S12 \\ S21 & S22 \end{bmatrix} \tag{1.29}$$

Thus, the elements of the S-matrix are the scattering parameters. An ideal isolator would be such that, the wave travels from left to right and is completely blocked in the opposite direction. Thus, an ideal isolator would have the S matrix

as shown below :

$$S = \begin{bmatrix} 0 & 0 \\ 1 & 0 \end{bmatrix} \tag{1.30}$$

Now, there are several internal reflections inside the isolator, which complicates the derivation of the scattering parameters, specifically for S11. A finite element analysis was carried out to plot the variation of these parameters with frequency. The frequency range is 10Hz to 10kHz. The plots below depicts this variation for different values of the control parameter 'd'. We can see from the plots that for low values of *'d'*, the isolator is close to being an ideal isolator.

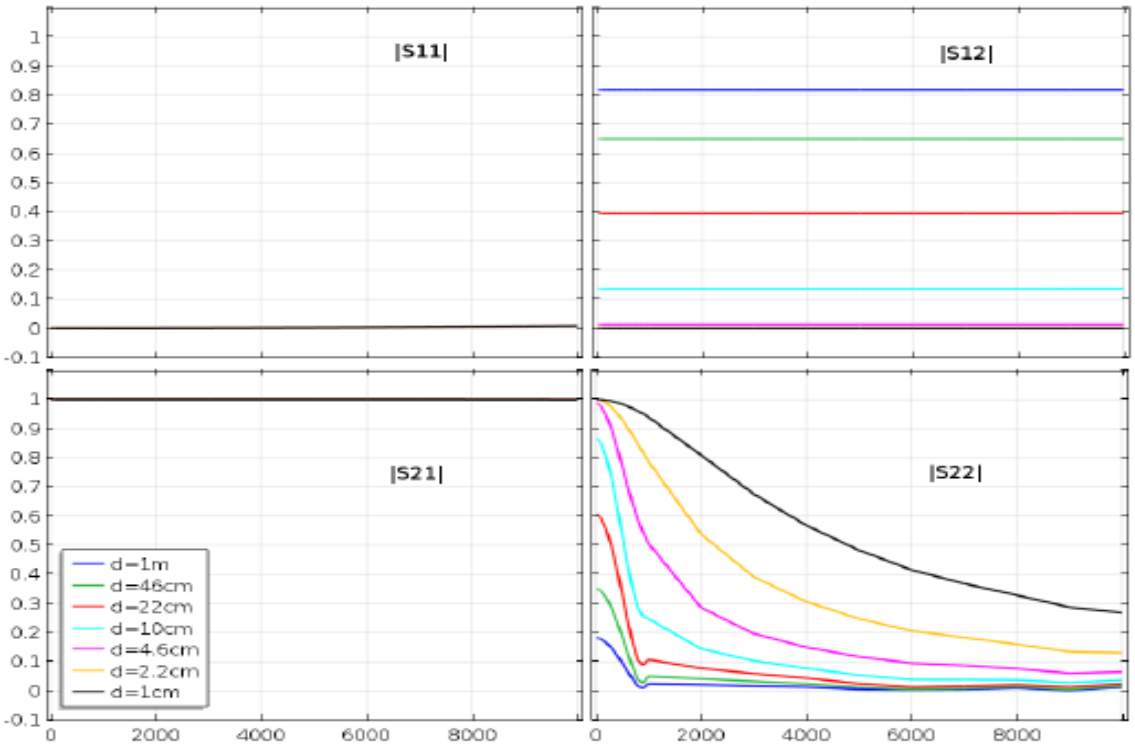

Figure 1.7: The x-axis is the frequency in Hz, and the y-axis are the respective scattering parameters. The plot compares the variation of these parameters for different values of the control parameter *'d'* (Karkar *et al.*, 2017)

As it can be seen from most of the papers reviewed above, there is lack of experiments which are not hard-wired and the frequency range in some cases is very limited. Our main focus in this dissertation is to obtain the experimental results for active control, which makes the system soft-wired, helped by the use of piezoelectric sensors and actuators.

1.6 Scope of the thesis

In this work, a dynamic control system is developed in order to control the propagation of pressure waves through a piezo cell and induce non-reciprocity into the system. Our system is constituted by a small acrylic cylinder, filled with water and having piezoelectric discs on both the bases. The results would be helpful in inducing one way actively controlled propagation over large frequency range in various real life applications such as sub-marines and aircrafts to name a few. This work also presents simulation results (using finite element analysis (FEA)) to compare it with the obtained experimental results.

Chapter 1 includes literature review of various reciprocity concepts and it's usefulness. It also cites many examples of researchers breaking this reciprocity by different methods, which have their limitations. The chapter 2 presents the theoretical backdrop of the piezo cell and it's control theory. An analogous electrical system of the given mechanical structure has been introduced to derive the simplified equations of motions. The chapter 3 presents the details of the system identification using impulse hammer method. It also provides details on the dynamic control

system implemented on the piezo cell using *LabVIEW* software. The chapter 4 provides details of the setting up of simulation in *ANSYS* Workbench for modal, harmonic and transient structural analysis of the piezo cell. The chapter 5 gives the various interpretations of the results obtained and mentions the future work needed to be done.

1.7 Summary

This chapter has presented and explained the concept of reciprocity and it's various applications and uses in the field of acoustics. Many different methods used by various researchers to break this reciprocity have been discussed in this chapter. It is found that the breaking of reciprocity in acoustics is far more challenging compared to other fields such as electromagnetics. Various mathematical formulations for the same have been discussed. It is also found that most of the systems being proposed for breaking the reciprocity are hard-wired and applicable to a limited frequency range, which is a huge drawback.

Chapter 2: Theory associated with Programmable Active Non-reciprocal Metamaterial cell

2.1 Basic structure of the acoustic cavity with piezodiaphragm

The basic structure of an active acoustic metamaterial cell *(AAMM)* has been depicted in the Figure (2.1). Corresponding to the mechanical structure, an analogous electrical structure has also been depicted in the various figures ahead.

As it can be seen in the electrical analogous circuit, the three components with the dashed-line ellipses enable the *AAMM* to have tunable and desirable characteristics. The capacitance C_s and the inductance L_p represent the passive components, while the capacitance $(-d_A^2 G)$ represents the active capacitance, which is generated as a result of the feedback control.

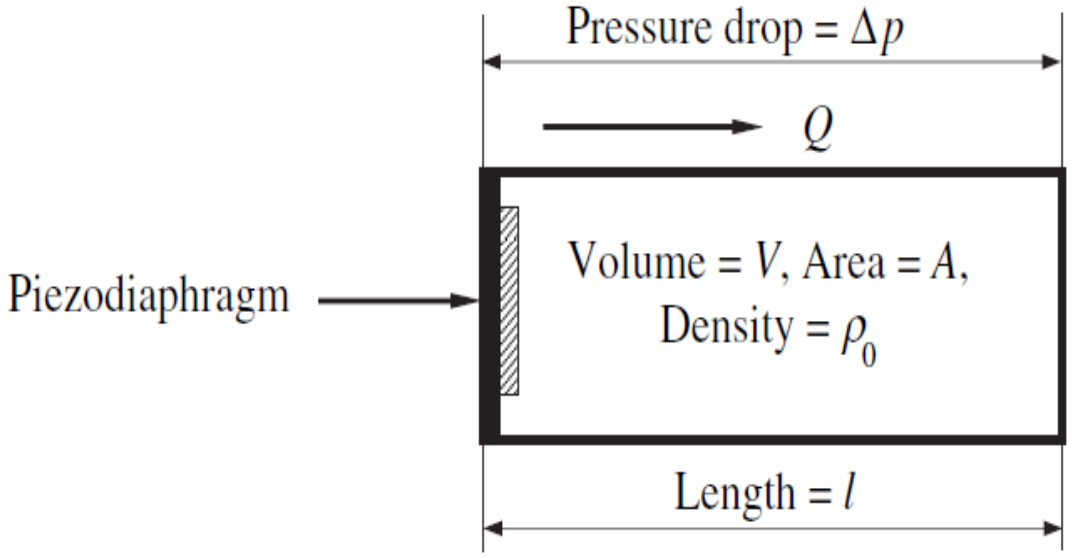

Figure 2.1: Mechanical structure of the *AAMM* (Baz, 2009)

We can write the basic equations of piezoelectric materials as shown.

$$\begin{Bmatrix} S \\ D \end{Bmatrix} = \begin{bmatrix} s^E & d \\ d & \epsilon \end{bmatrix} \begin{Bmatrix} T \\ E \end{Bmatrix} \tag{2.1}$$

where, $S =$ strain, $D =$ electrical displacement, $T =$ stress, $E =$ electrical field, $d =$ piezoelectric strain coefficient, $\epsilon =$ permittivity and $s^E =$ compliance. We can also rewrite the above equations as :

$$\begin{Bmatrix} \Delta Vol \\ q \end{Bmatrix} = \begin{bmatrix} C^d & d_A \\ d_A & 1/Z_p s \end{bmatrix} \begin{Bmatrix} \Delta P_p \\ V_p \end{Bmatrix} \tag{2.2}$$

where, $q =$ electrical charge, $\Delta Vol =$ change in diaphragm volume, $\Delta P_p =$ pressure across the piezodiaphragm, $V_p =$ voltage, $C_D =$ diaphragm compliance and $Z_p =$ impedance of piezodiaphragm and other passive elements, which is given by

$$Z_p = \frac{L_p s}{(1 + (L_p C_p C_s s^2)/(C_p + C_s))} \tag{2.3}$$

where, C_p = capacitance of piezodiaphragm ($= A\epsilon/t$) with t = thickness of diaphragm, A = area of diaphragm, L_p = shunted inductance in parallel with piezodiaphragm, C_s = capacitance in series with the piezodiaphragm.

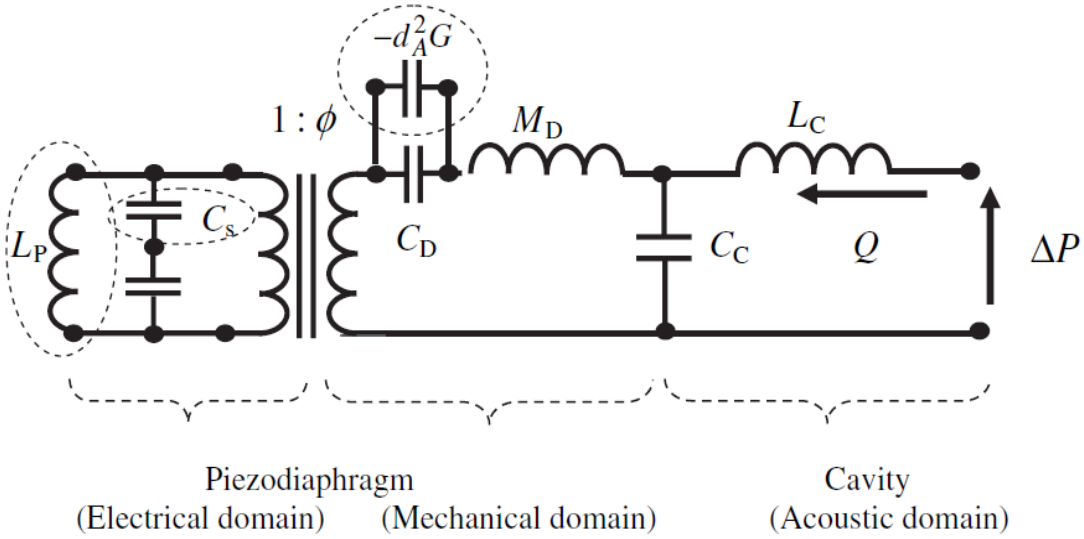

Figure 2.2: Electrical analogue of the *AAMM* (Baz, 2009)

Also, as the piezoelectric diaphragm produces displacement as a result of voltage, and vice-versa, it can be used as a self-sensing actuator. For a piezo-circuit which has been short-circuit, the second row of the matrix equation gives :

$$q = d_A \Delta P_p \tag{2.4}$$

Then, voltage feedback control system can be made by applying voltage V_p to the piezodiaphragm, using the charge q as thew feedback, as shown :

$$V_p = -Gd_A\Delta P_p \tag{2.5}$$

Where, G = Control feedback gain.

Also, the first row of the matrix equation expands to give :

$$\Delta Vol = (C_D - d_A^2 G)(\Delta P_p) = C_{DC}\Delta P_p \tag{2.6}$$

where, C_{DC} = closed-loop compliance of piezodiaphragm.

In the above equation, we can see that C_{DC} is formed by the parallel combination of of passive compliance of the diaphragm (C_D) and an active capacitance (-d_A^2G). The following figure depicts a simplified analogous electrical circuit of the AAMM.

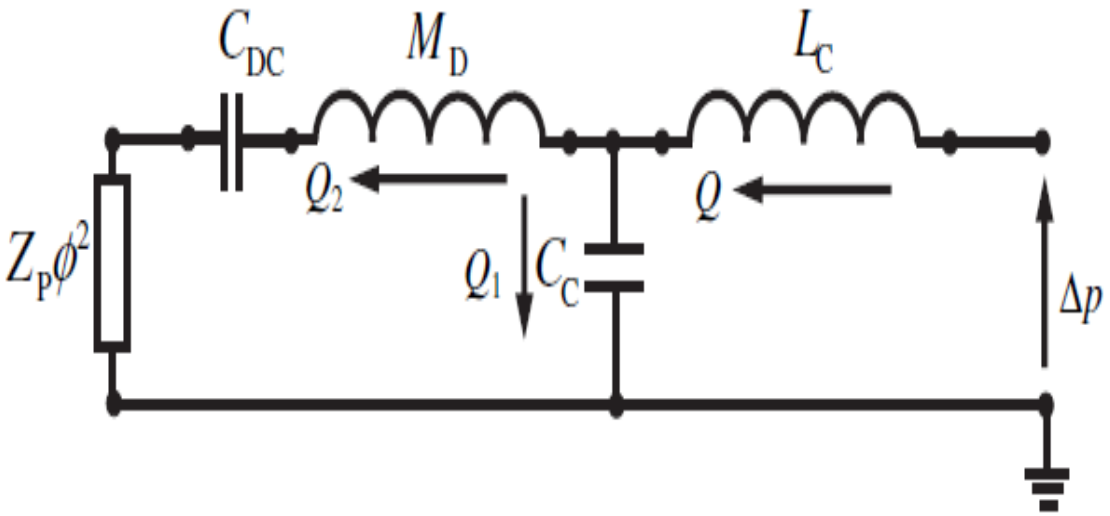

Figure 2.3: Simplified electrical analogue of the *AAMM* (Baz, 2009)

Also, the transfer function of the closed-loop system, relating the pressure drop

(ΔP) to the flow velocity u is given as :

$$\frac{\Delta P}{l} = -\rho_0[1 + \frac{C_{DC}T + 1}{L_C s^2(C_{DC} + C_C[C_{DC}T + 1])}]su \tag{2.7}$$

where,

$$T = M_D s^2 + Z'_p s \tag{2.8}$$

where,

$$Z'_P = Z_p \phi^2 \tag{2.9}$$

2.2 Active nonreciprocal acoustic metamaterials *(ANAM)* using a switching controller

The flow of acoustic energy inside the acoustic cavity can be controlled by application of proper control voltages on the electrical boundaries represented by the piezo bimorphs on both sides of the cell. This control voltage can be generated by connecting a shunted network of switching resistors, which are nonlinearly activated. By selecting the correct ratio of the values of these resistors, nonreciprocal characteristics of the *ANAM* cell can be demonstrated. A lumped-parameter model of the *ANAM* cell has thus been introduced.

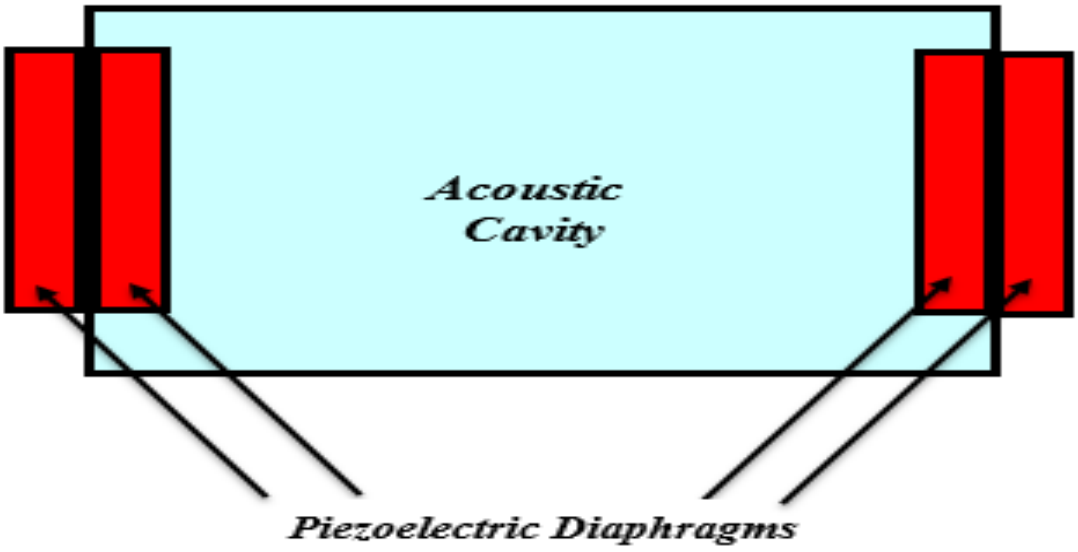

Figure 2.4: Basic structure of the *ANAM*

The structure and construction of the *ANAM* cell has been depicted in Figure (2.4). It is a cylinder having an acoustic cavity, and piezo bimorphs, which act as sensors to measure and monitor the pressure inside the cell. The piezo bimorphs on the outer surface of the *ANAM* cell generate the appropriate control voltages in order to demonstrate a control strategy.

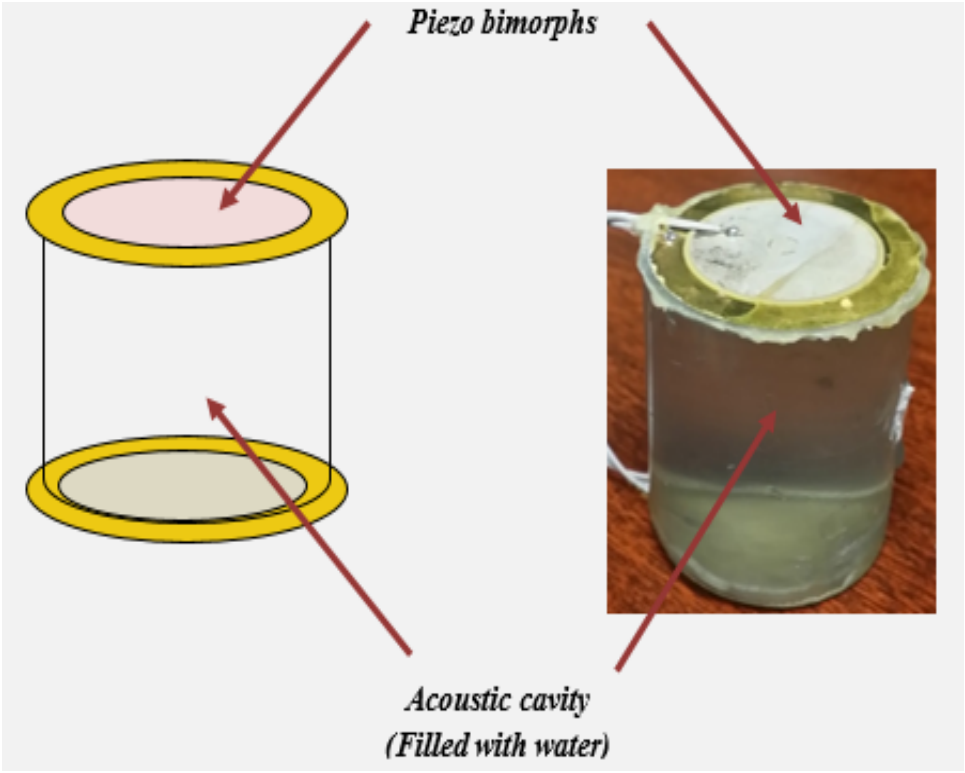

Figure 2.5: Prototype of the *ANAM* cell

The *ANAM* cell has various pressure sensors inside the cell to monitor the pressure gradient across the cell, as the acoustic waves propagate through the longitudinal direction of the cell. The piezo-bimorph on the left side is excited by incident pressure, which generates a pressure wave which travels across the longitudinal direction of the cell. The pressure is measured on the right piezo bimorph. This pressure activates the switching network to generate the required control voltage. The problem with most of the systems out there is, that the direction of non-reciprocity cannot be reversed as the system is hard-wired. But, in this case, we can implement the switching network on the left side and reverse the direction of non-reciprocity.

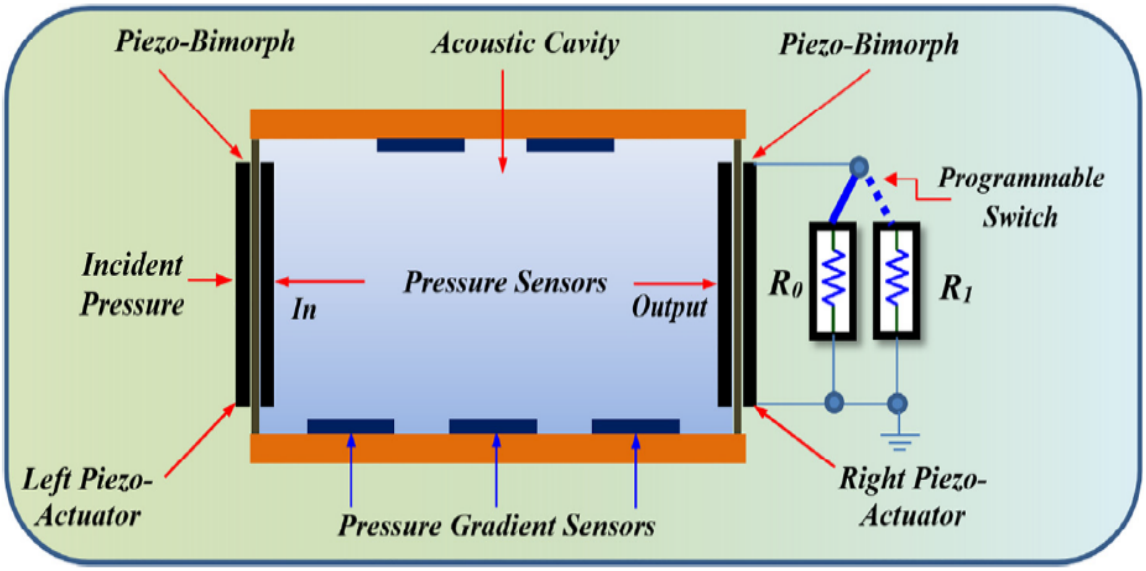

Figure 2.6: Basic structure of the *ANAM* cell (Baz, 2018)

In order to fully predict the dynamic characteristics of the *ANAM* cell, an analogous electrical circuit, representing the *ANAM* cell is constructed. If the dimensions of the *ANAM* cell are much smaller compared to the smallest wavelength of the acoustic waves propagating inside the cell, then the analogous model can accurately predict the performance of the *ANAM* cell.

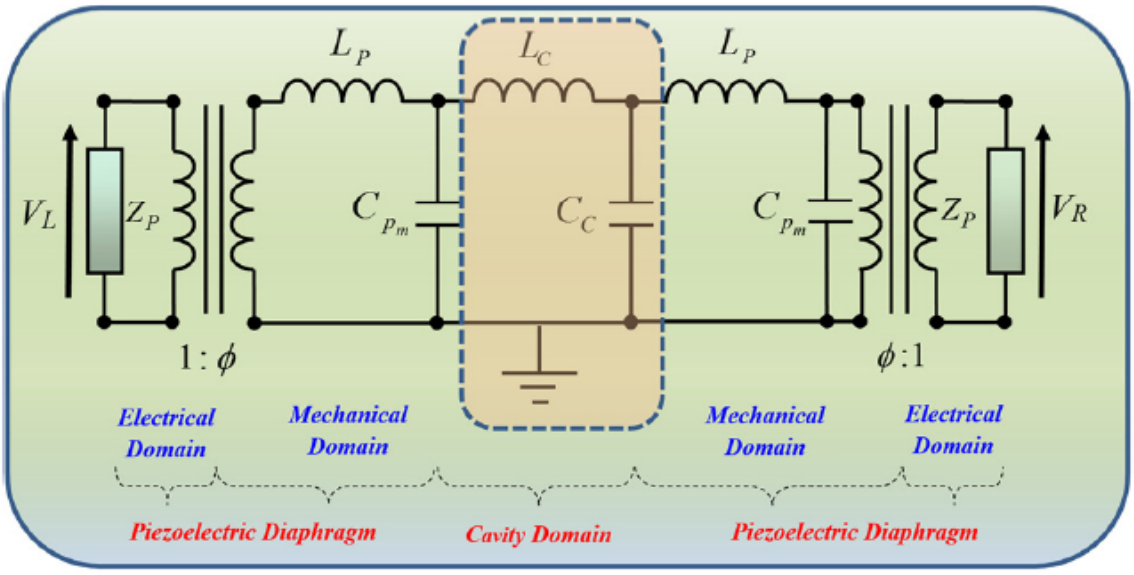

Figure 2.7: Electrical circuit analogue of the *ANAM* cell (Baz, 2018)

The figure above represents the 1-D model of the cell. The stiffness and mass of the acoustic cavity of the cell are represented by the capacitance C_c and the inductance L_c respectively. Now, as the piezo bimorphs are a combination/coupling of electrical and mechanical parts, the circuit has split the piezo bimorphs into electrical and mechanical components which have been coupled by a transformer which has a transformation ratio of 1:ϕ, with ϕ depicting the acoustic pressure/voltage transformation factor. The mechanical part of the piezo bimorph has it's mass and stiffness, which is represented by the inductance L_p and the capacitance C_{pm} respectively. It is coupled with the electrical part of the piezo bimorph by a transformer. Now, any shunted electric network, which has been connected to the *ANAM* cell in order to construct a control system, is represented by the electric impedance of the piezo bimorph Z_p.

2.3 Active Control of the *ANAM* Cell

Figure (2.8) represents an idealized version of the ANAM cell, in which, the quick dynamic characteristics of the piezo bimorphs have been neglected compared to the slow dynamic characteristics of the acoustic cavity. This neglection helps in getting a better perspective of the idealized version of the cell.

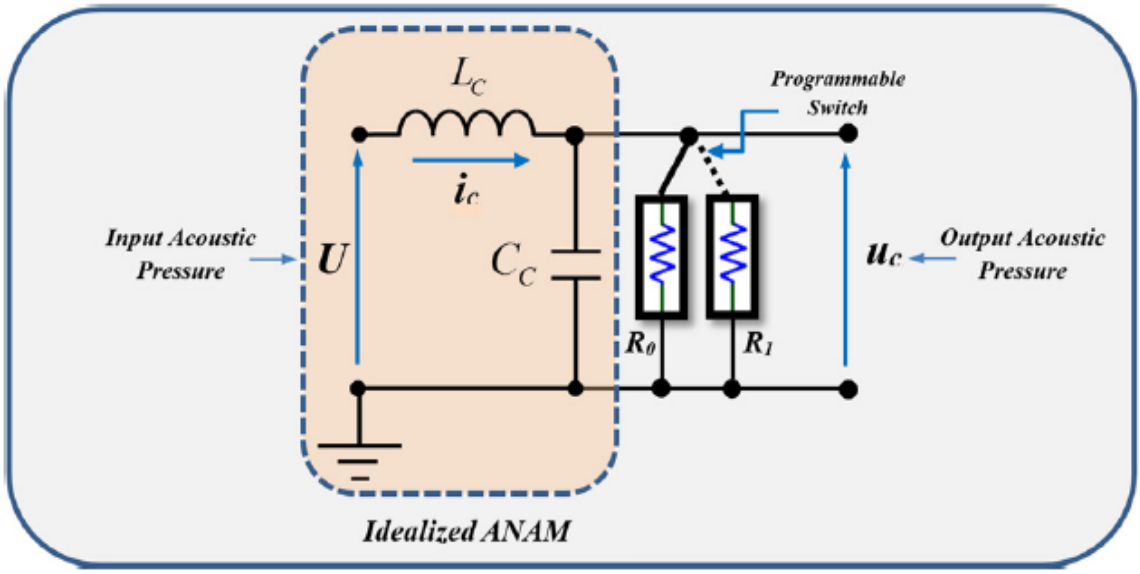

Figure 2.8: An idealized *ANAM* cell (Baz, 2018)

The control system has been implemented using the Switching Mode Control *(SMC)* strategy on the idealized *ANAM* cell. The control system consists of a programmable controller which switches between the two shunted resistors R_1 and R_0. The state-space system representing the dynamic characteristics of the *ANAM* cell is shown below :

$$\frac{d}{dt}\begin{Bmatrix} i_c \\ u_c \end{Bmatrix} = \begin{bmatrix} 0 & \frac{-1}{L_c} \\ \frac{1}{C_c} & \frac{-1}{RC_c} \end{bmatrix} \begin{Bmatrix} i_c \\ u_c \end{Bmatrix} + \begin{Bmatrix} \frac{1}{L_c} \\ 0 \end{Bmatrix} U \tag{2.10}$$

Where R (non-linear shunted resistance) assumes the value of either R_0 or R_1 depending upon the switching controller. The above equations is rewritten as :

$$\frac{d}{dt}\begin{Bmatrix} u_c \\ \dot{u}_c \end{Bmatrix} = \begin{bmatrix} 0 & 1 \\ \frac{-1}{C_c L_c} & \frac{-1}{RC_c} \end{bmatrix} \begin{Bmatrix} u_c \\ \dot{u}_c \end{Bmatrix} + \begin{Bmatrix} 0 \\ \frac{1}{L_c C_c} \end{Bmatrix} U \tag{2.11}$$

which is similar to :

$$\dot{X} = AX + BU \tag{2.12}$$

Where,

$$X = \begin{Bmatrix} u_c \\ \dot{u}_c \end{Bmatrix}, \quad A = \begin{bmatrix} 0 & 1 \\ \frac{-1}{C_c L_c} & \frac{-1}{RC_c} \end{bmatrix}, \quad B = \begin{Bmatrix} 0 \\ \frac{1}{L_c C_c} \end{Bmatrix} \tag{2.13}$$

Thus, the switching between R_1 and R_0 is done by the switching line σ :

$$\sigma = \dot{u}_c + \alpha u_c = \begin{Bmatrix} \alpha & 1 \end{Bmatrix} X, \ \alpha > 0 \tag{2.14}$$

A Lyapunov function V is defined in order to monitor the stability of the switching controller :

$$V = \frac{1}{2}\sigma^2 = \frac{1}{2}X^T P X \tag{2.15}$$

where,

$$P = \begin{bmatrix} \alpha^2 & \alpha \\ \alpha & 1 \end{bmatrix} \tag{2.16}$$

As seen above, P is a symmetric matrix. Also, the above mentioned Lyapunov function is quadratic in nature, and it has a global minimum at $X = 0$, which is where the system achieves stable equilibrium. Stability can be confirmed by ensuring that $\dot{V}$ (rate of decay of the system's energy) is strictly negative :

$$\dot{V} = \sigma\dot{\sigma} = \sigma(\ddot{u}_c + \alpha\dot{u}_c) < 0 \tag{2.17}$$

We get the equation $\dot{u}_c$ = -αu_c from the switching line equation : $\sigma = \dot{u}_c + \alpha u_c = 0$

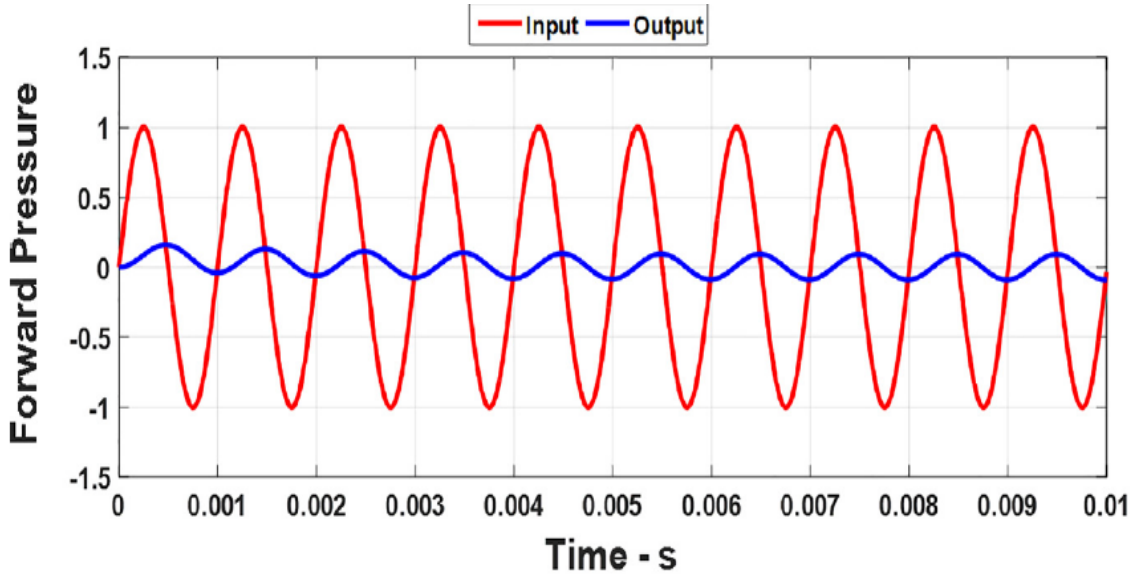

Figure 2.9: Attenuation characteristics of the *ANAM* cell with α (slope of the switching line) = 1E6 (Baz, 2018)

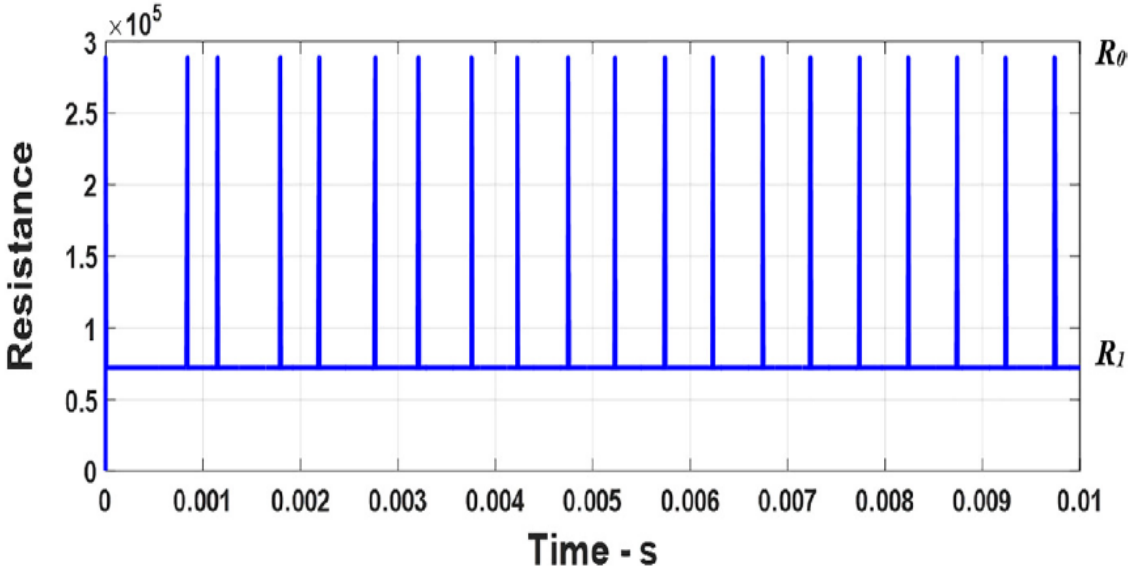

Figure 2.10: Resistance characteristics of the *ANAM* cell with α (slope of the switching line) = 1E6 (Baz, 2018)

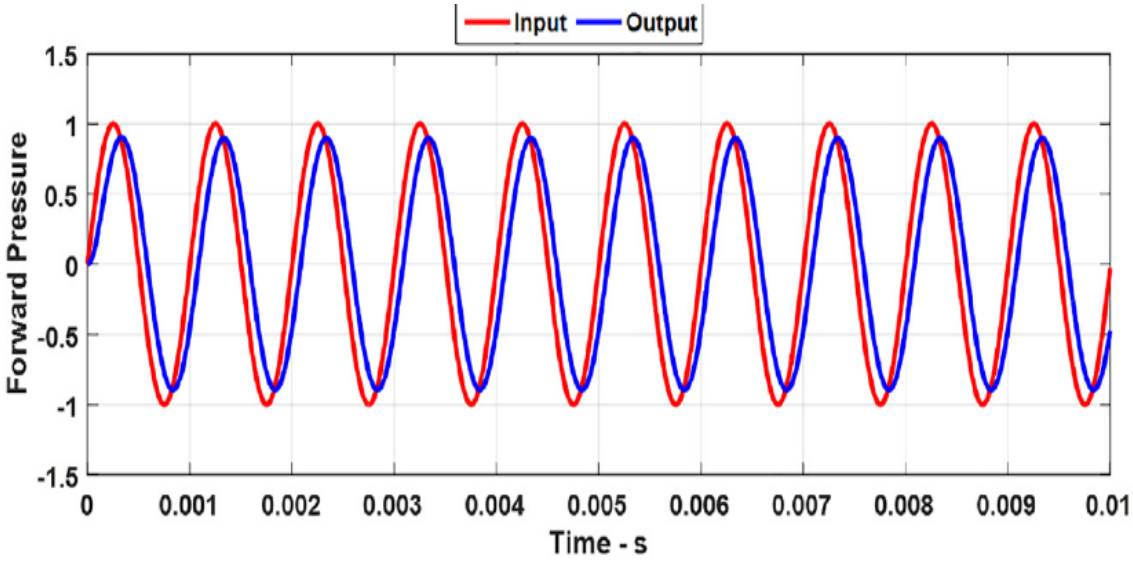

Figure 2.11: Attenuation characteristics of the *ANAM* cell with α (slope of the switching line) = 0.13E6 (Baz, 2018)

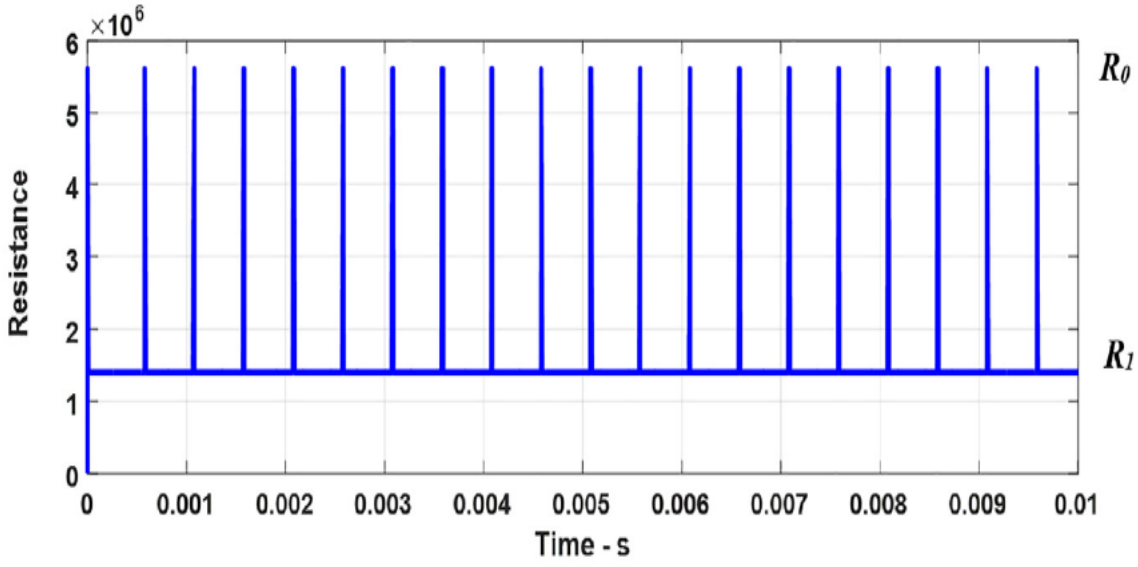

Figure 2.12: Resistance characteristics of the $ANAM$ cell with α (slope of the switching line) = 0.13E6 (Baz, 2018)

Furthermore, we can write the system's energy decay as :

$$\dot{V} = \sigma(-u_c/C_C L_C + \alpha u_c/C_C R + U/C_C L_C + \alpha(-\alpha u_c)) < 0 \tag{2.18}$$

Now, if $U_{max} = \gamma u_c$ with $\gamma > 1$, then, we can write :

$$\implies \dot{V} < -(\alpha^2 - (\gamma - 1)/(C_C L_C) - \alpha/C_C R)(\sigma u_c) \tag{2.19}$$

From above, we can see that, stability is achieved in switching when $\dot{V} < 0$ is satisfied. Hence, the following two laws must be satisfied :

Law 1 : $\sigma u_c > 0$, then

$$R = R_0 > \alpha/(C_C(\alpha^2 - ((\gamma - 1)/(C_C L_C)))) = \alpha/C_C\delta \tag{2.20}$$

$$\implies R_0 = \alpha\beta/C_C\delta \tag{2.21}$$

$$\implies \dot{V} < 0 \tag{2.22}$$

Law 2 : $\sigma u_c < 0$, then

$$R = R_1 < \alpha/(C_C(\alpha^2 - ((\gamma - 1)/(C_C L_C)))) = \alpha/C_C\delta \tag{2.23}$$

$$\implies R_1 = \alpha/\beta C_C\delta \tag{2.24}$$

$$\implies \dot{V} < 0 \tag{2.25}$$

where,

$$\delta = \alpha^2 - \frac{\gamma - 1}{C_C L_C}, \quad \beta > 1 \tag{2.26}$$

It is important to be note that in order to implement this switching controller successfully, the accurate measurement of u_c and/or it's derivative is required, which can be obtained from the piezo sensor bimorph.

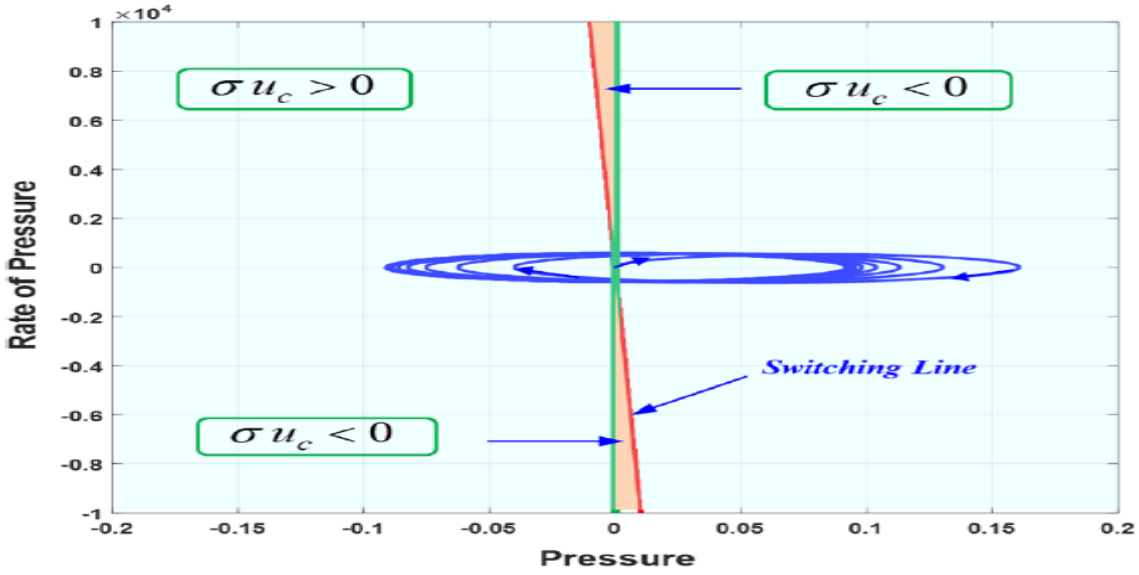

Figure 2.13: Phase plane characteristics of the *ANAM* cell with α (slope of the switching line) = 1E6 (Baz, 2018)

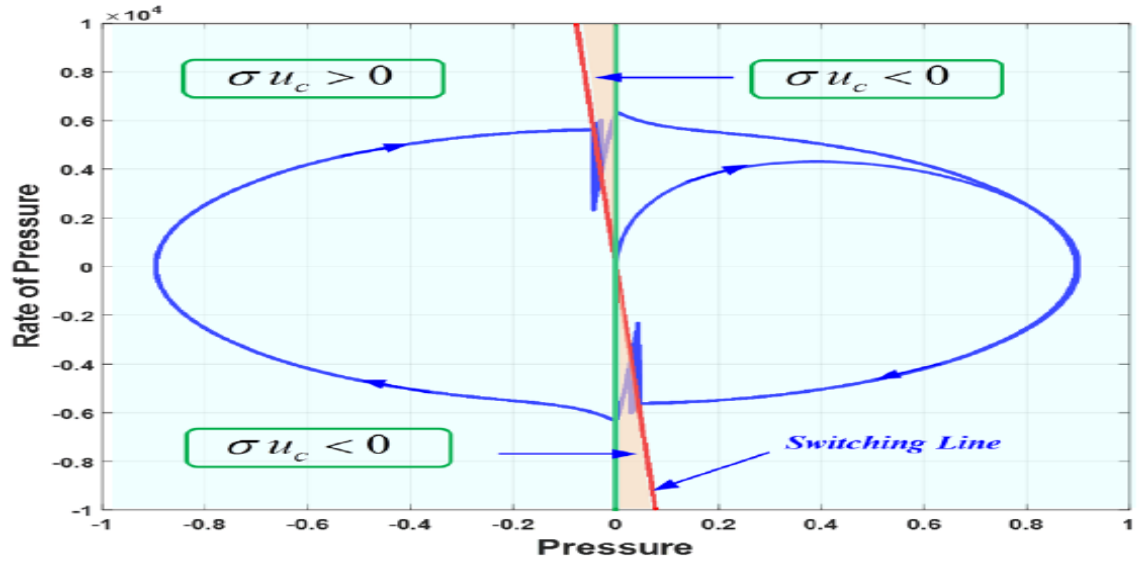

Figure 2.14: Phase plane characteristics of the *ANAM* cell with α (slope of the switching line) = 0.13E6 (Baz, 2018)

2.4 *ANAM* Static Controller

Now, from the state-space equation for the *ANAM* cell from the previous section, we can represent the dynamics of the cell in the following way :

$$\frac{d}{dt}\begin{Bmatrix} u_c \\ \dot{u}_c \end{Bmatrix} = \begin{bmatrix} 0 & 1 \\ \frac{-1}{C_c L_c} & \frac{-1}{RC_c} \end{bmatrix} \begin{Bmatrix} u_c \\ \dot{u}_c \end{Bmatrix} + \begin{Bmatrix} 0 \\ \frac{1}{L_c C_c} \end{Bmatrix} U + \begin{Bmatrix} 0 \\ \frac{1}{L_c C_c} \end{Bmatrix} f_c \tag{2.27}$$

$$\implies \ddot{u}_c + 2\zeta_c \omega_c \dot{u}_c + \omega_c^2 u_c = \omega_c^2 U + \omega_c^2 f_c \tag{2.28}$$

where, $\omega_c^2 = 1/(L_c C_c)$, $2\zeta_c\omega_c = R_c/L_c$, $\zeta_c = R_c C_c^{1/2}/(2L_c^{1/2})$, U = Excitation, u_c = Output Pressure

A static controller can be designed as shown in Figure (2.15). After exciting the left sided piezo bimorph of the *ANAM* cell, $\dot{u}_c$ needs to be measured at the outer piezo bimorph on the right side. This measured signal goes into the software, and after performing the required mathematical operations on it, a new feedback signal f_c is generated, the negative of which is sent to the left sided piezo bimorph.

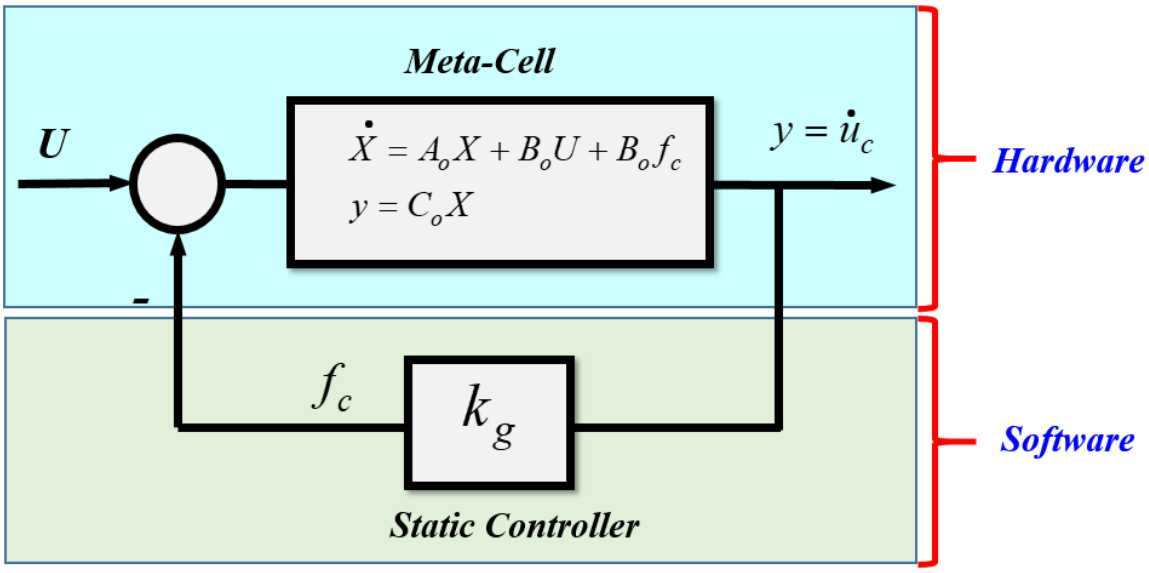

Figure 2.15: Static controller diagram

Now, in the above equation, if :

$$f_c = -K_v \dot{u}_c - K_p u_c \tag{2.29}$$

where, K_v = Velocity Feedback Gain, K_p = Proportional Feedback Gain

With the feedback, the equation of motion can be rewritten as :

$$\ddot{u}_c + (2\zeta_c \omega_c + \omega_c^2 K_v)\dot{u}_c + (\omega_c^2 + \omega_c^2 K_p)u_c = \omega_c^2 U \tag{2.30}$$

In the above equation, the term '$\omega_c^2 K_v$' represents damping, while the term '$\omega_c^2 K_p$' represents the stiffness. Thus, the static controller enhances the damping as well as stiffness of the system. It is also seen that the structure of the closed-loop system remains similar to that of the open-loop system.

2.5 *ANAM* Dynamic Controller

The following figure represents the dynamic controller :

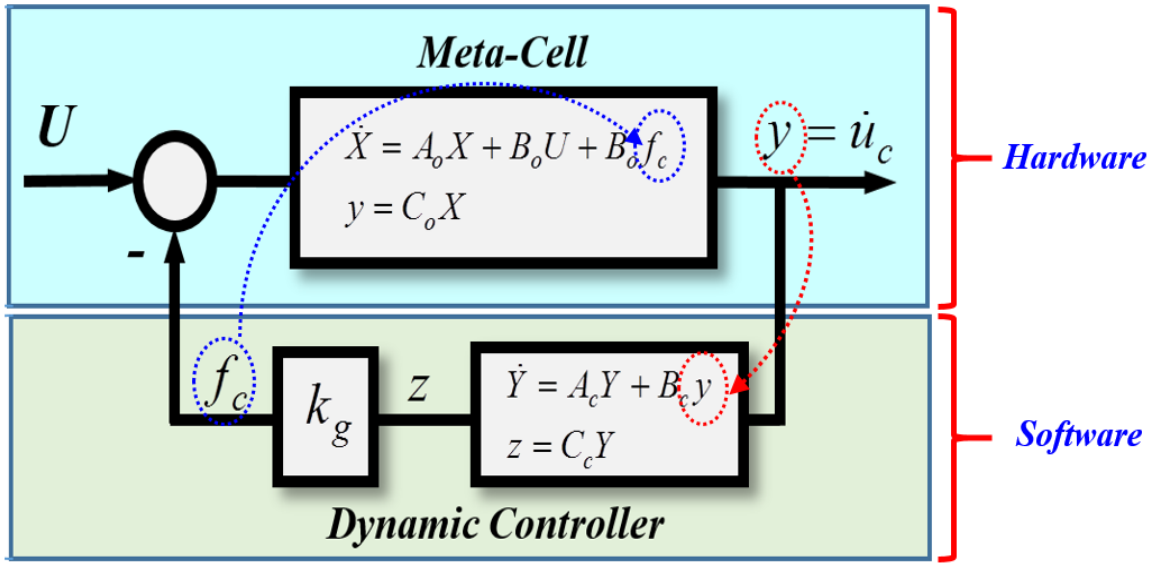

Figure 2.16: Dynamic controller diagram

Now, from the previous uncontrolled equation of motion, let :

$$f_c = K_g \dot{z} \tag{2.31}$$

where, z satisfies the following dynamic control equation :

$$\ddot{z} + 2\zeta_y \omega_y \dot{z} + \omega_y^2 z + K_g \omega_c^2 \dot{u}_c = 0 \tag{2.32}$$

Thus, the above equation represents the equation for the controller, where the term '$K_g \omega_c^2 \dot{u}_c$' represents coupling with the meta cell. So, the equation of motion for the cell is given as :

$$\ddot{u}_c + 2\zeta_c\omega_c\dot{u}_c - \omega_c^2 K_g\dot{z} + \omega_c^2 u_c = \omega_c^2 U \tag{2.33}$$

Combining these two equations, we can write a matrix equation as follows :

$$\begin{Bmatrix} \ddot{u}_c \\ \ddot{z} \end{Bmatrix} + \begin{bmatrix} 2\zeta_c\omega_c & 0 \\ 0 & 2\zeta_z\omega_z \end{bmatrix} \begin{Bmatrix} \dot{u}_c \\ \dot{z} \end{Bmatrix} + \begin{bmatrix} 0 & -K_g\omega_c^2 \\ K_g\omega_c^2 & 0 \end{bmatrix} \begin{Bmatrix} \dot{u}_c \\ \dot{z} \end{Bmatrix} + \begin{bmatrix} \omega_c^2 & 0 \\ 0 & \omega_z^2 \end{bmatrix} \begin{Bmatrix} u_c \\ z \end{Bmatrix} = \begin{Bmatrix} 0 \\ \omega_c^2 \end{Bmatrix} U \tag{2.34}$$

We can see that the structure of this closed-loop system is completely different from that of the open-loop system.

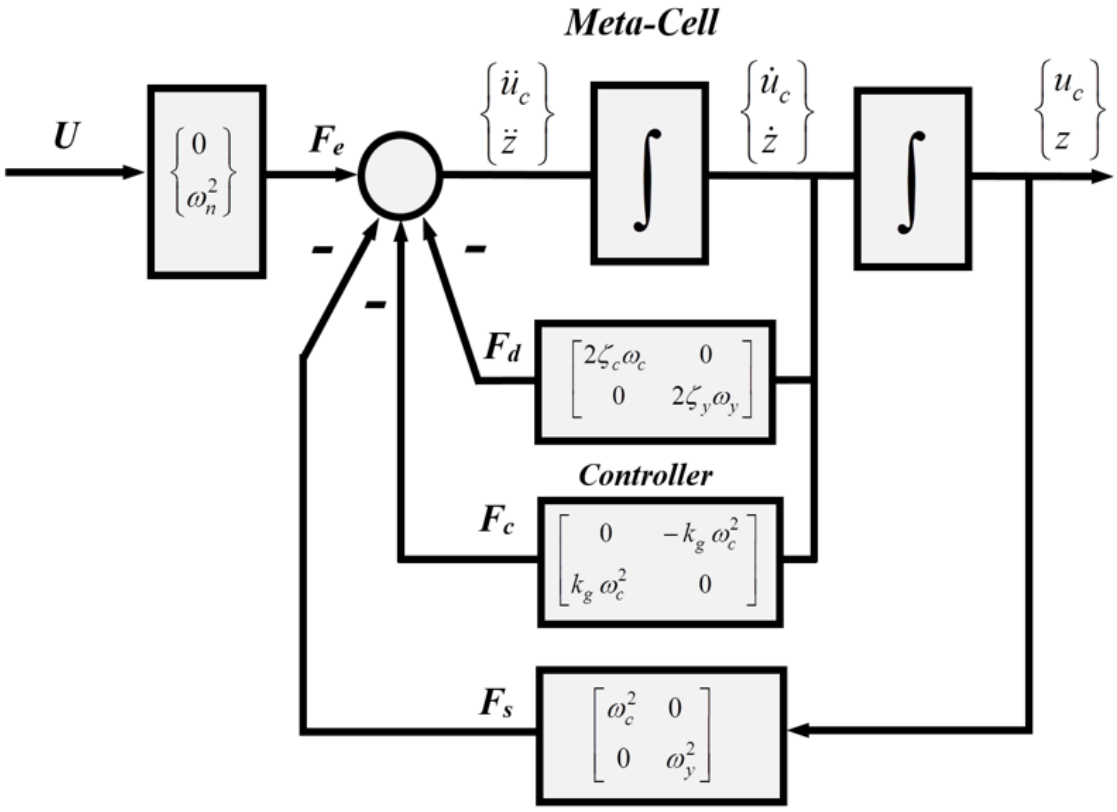

Figure 2.17: Dynamic controller schematic diagram breakdown

Now, to monitor the stability of this dynamic system, we define a Lyapunov function V, which is a combination of the energies of the cell and the dynamic controller, such that :

$$V = (\frac{1}{2}\dot{u}_c^2 + \frac{1}{2}\omega_c^2 u_c^2) + (\frac{1}{2}\dot{z}^2 + \frac{1}{2}\omega_z^2 z^2) \tag{2.35}$$

Now, the derivative of this function, which represents the time-rate of decay of the energy of the system, is given as :

$$\begin{aligned} \dot{V} = &-2\zeta_c\omega_c\dot{u}_c^2 + k_g\omega_c^2\dot{z}\dot{u}_c - \omega_c^2\dot{u}_c\dot{u}_c + \omega_c^2\dot{u}_c\dot{u}_c \\ &-2\zeta_z\omega_z\dot{z}^2 - k_g\omega_c^2\dot{z}\dot{u}_c - \omega_z^2\dot{z}\dot{z} + \omega_z^2\dot{z}\dot{z} < 0 \end{aligned} \tag{2.36}$$

$$\implies \dot{V} = -2\zeta_c\omega_c\dot{u}_c^2 - 2\zeta_z\omega_z\dot{z}^2 < 0 \tag{2.37}$$

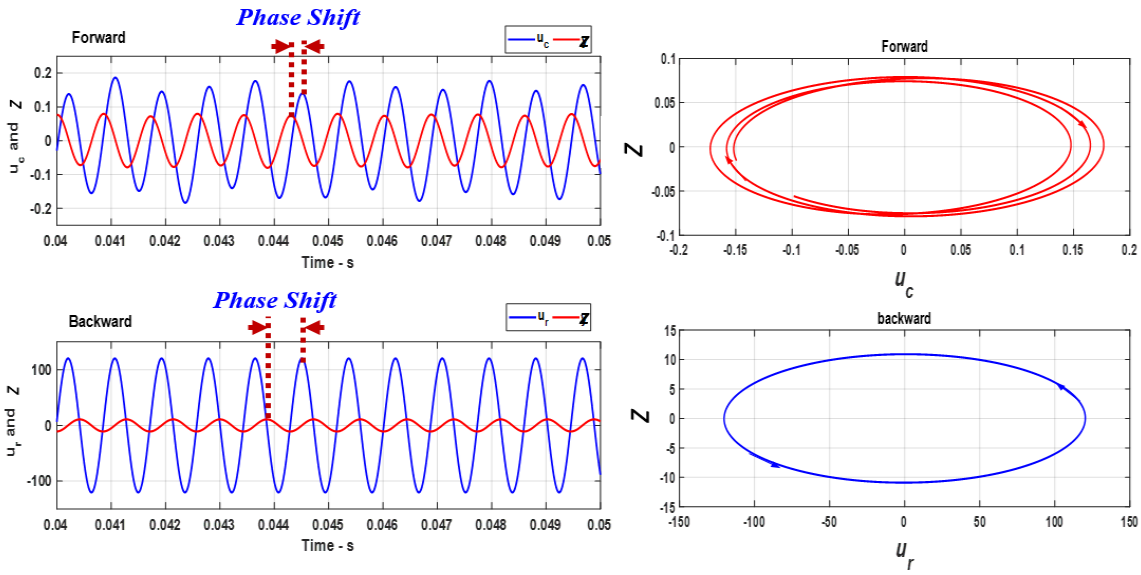

Figure 2.18: Phase shift characteristics with forward and backward control

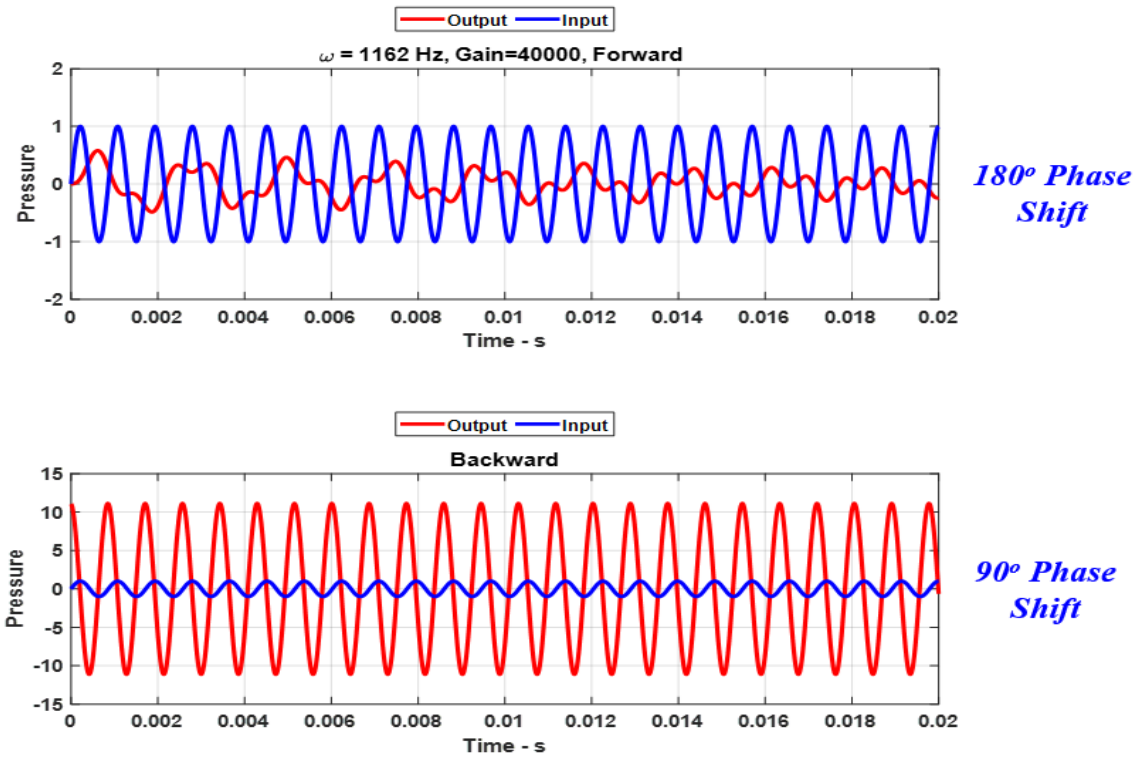

Figure 2.19: Various phase shifts achieved with the dynamic controller

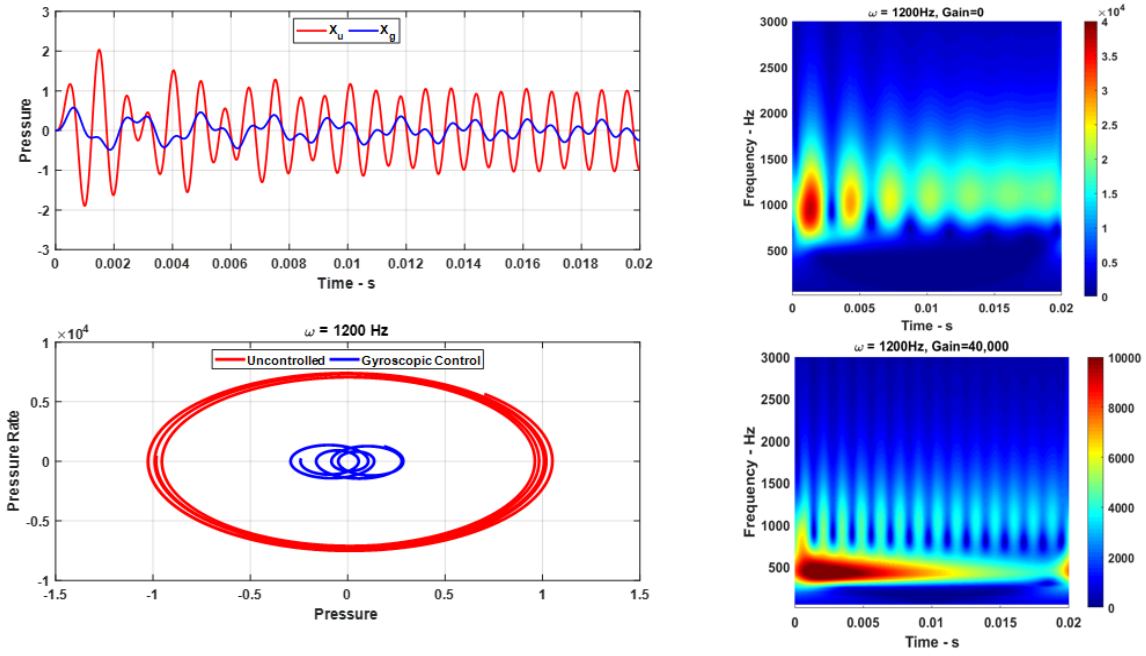

Figure 2.20: Pressure and frequency characteristics with dynamic control

2.6 Summary

This chapter has introduced the basic structure of our proposed system, which is an acrylic cylindrical cell, filled with water and having piezo boundaries. The mathematical equations pertaining to piezo material (being used for boundary control) have been discussed. An electrical analogous system of the mechanical (piezo cell) system has been introduced for better understanding and the ease of derivation of the equation of motions. The idea behind the active switching control of the piezo cell has been introduced. This chapter also introduces the equations and the mathematical calculations behind the design of static and dynamic controller for the active control of piezo cell. After introducing the equations, the results for control have been plotted and presented, after assuming values of various parameters for the required calculations. These results include the time response and the corresponding phase plane plots.

Chapter 3: Experimental Setup for Active Acoustic Metamaterial Cell

3.1 Impulse Hammer Experiment

A system identification process is carried out to identify the system characteristics and behavior, in order to design an appropriate control system. The system identification of the piezo cell is carried out using the impulse response approach.

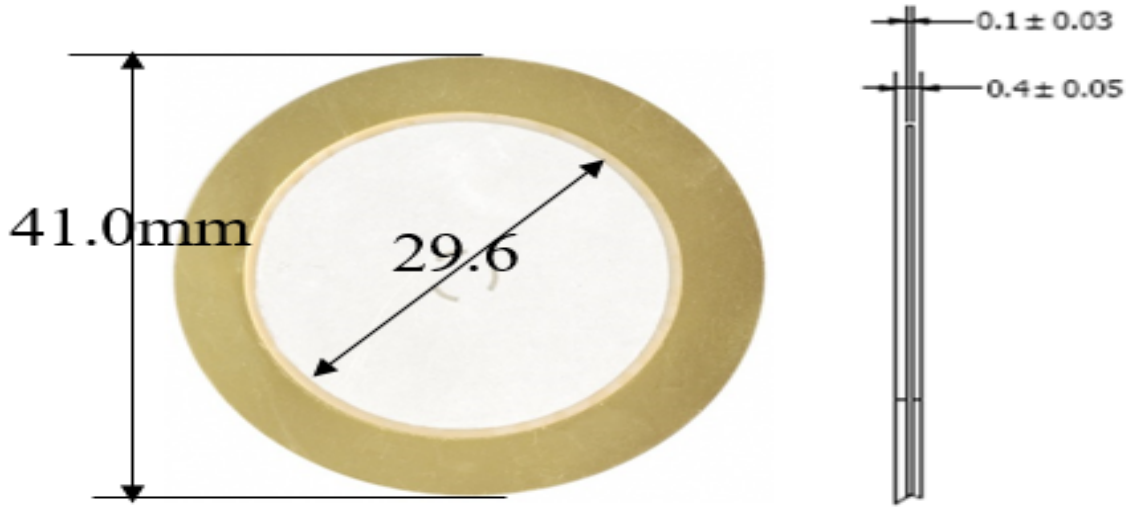

Figure 3.1: Dimensions of the piezo film

Piezo Material	PZT4
Frequency	1.3kHz
Capacitance @ Frequency	150000pF @ 1kHz
Voltage - Input, Max	30V p-p
Impedance	200 Ohm
Diameter	1.61" Dia (41mm)

Figure 3.2: Properties of the piezo film used

An impulse hammer is employed to apply impulse input to the piezo-actuator 1 of the structure. The impulse signal was captured using an analyzer. The output at the piezo-sensor 2 of the structure is monitored. The impulse force generated using the impulse hammer and the corresponding response have been shown in Figures (3.3) and (3.4) repectively.

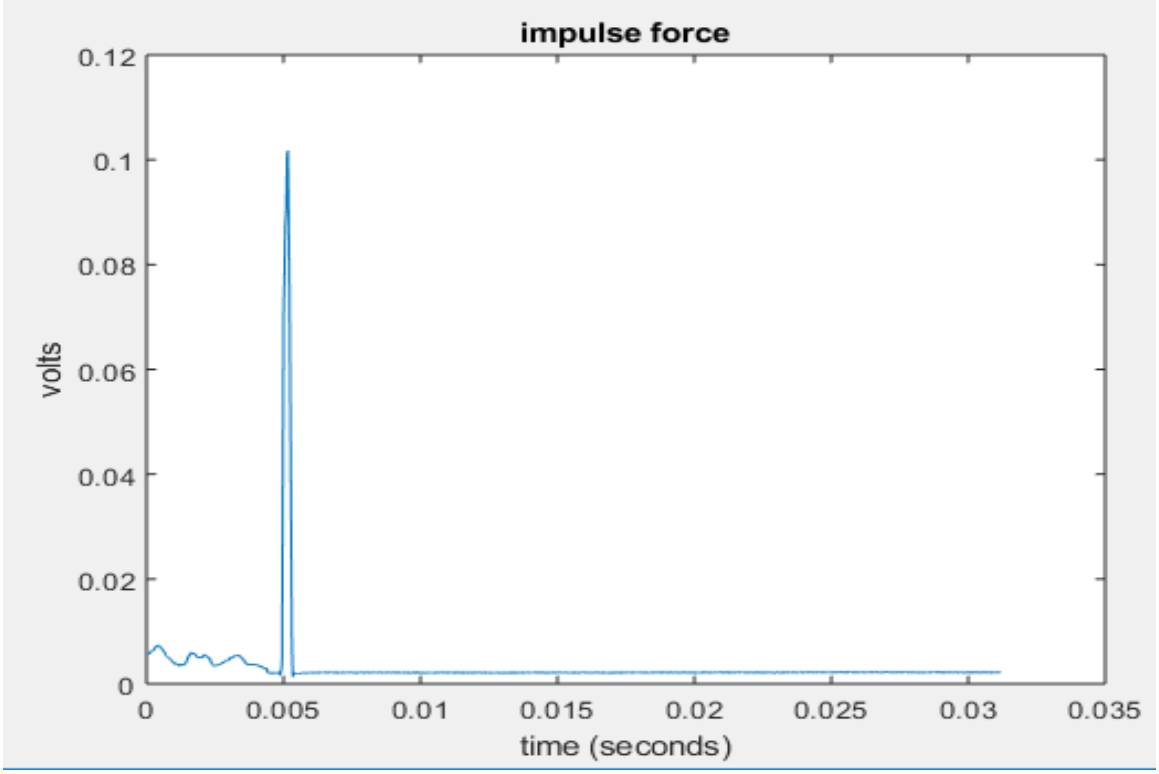

Figure 3.3: The Impulse Force generated by the Impulse Hammer, recorded by the Analyzer

The analyzer could capture the data at a sampling rate of 3E-5 seconds. Thus, we have the input data (impulse force), output data (respsonse at piezo-sensor 2) and the sampling time (3E-5 seconds). Using this information, system identification process ahs been carried out, which is described in the following section.

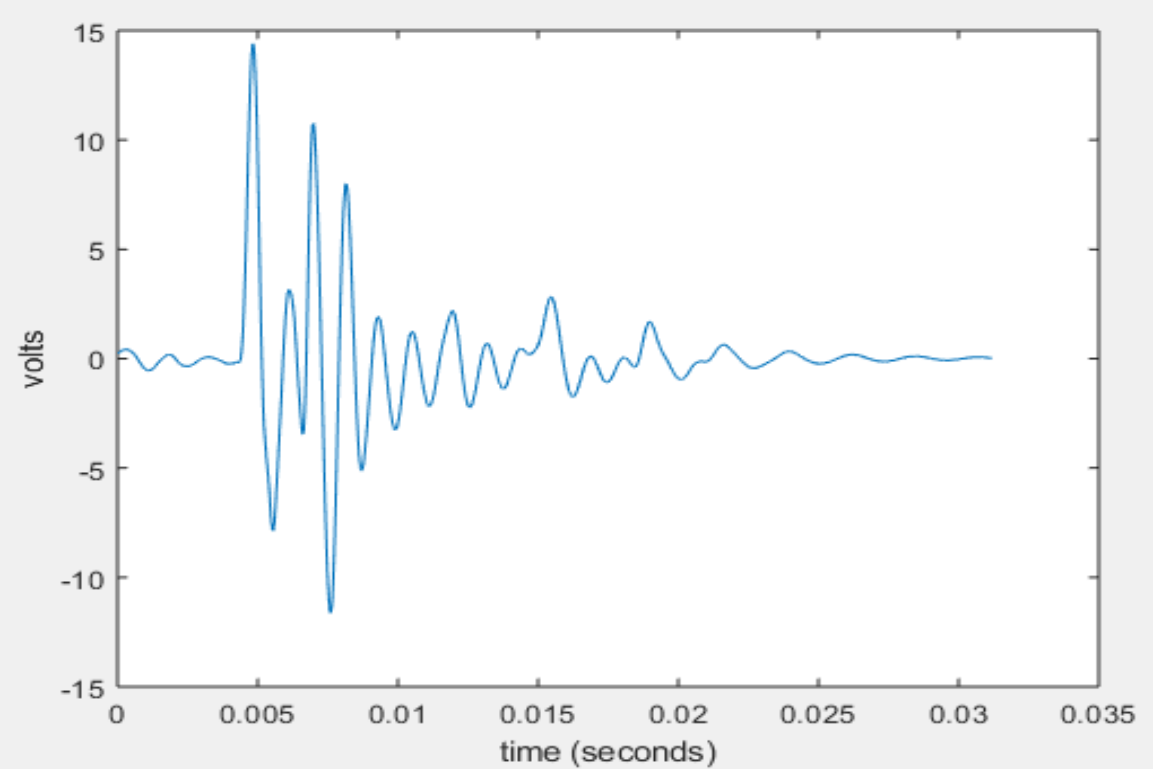

Figure 3.4: The Impulse response, as measured by the Analyzer on the piezo-sensor 2 of the active acoustic metamaterial cell

3.2 System Identification

Two sets of input and output data are used in the system identification using the system identification toolbox in *MATLAB*.

Now, the system identification toolbox is initiated by, the command *"ident"* in *MATLAB*. Once the toolbox is activated, the input and output data are imported into the toolbox, as shown in Figure (3.5) below.

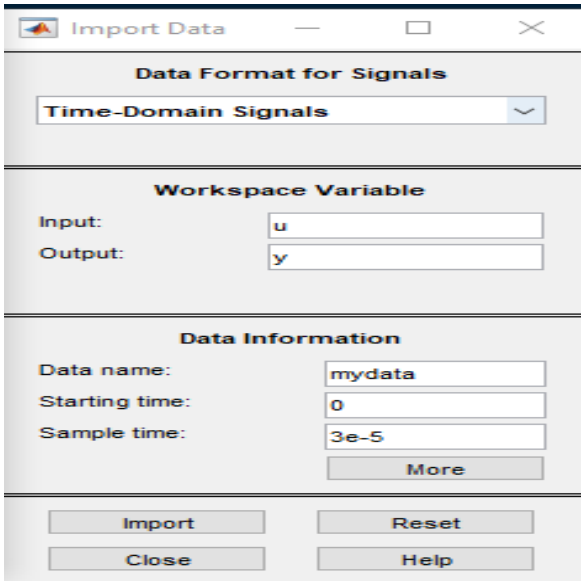

Figure 3.5: Assignment of variables in the system identification toolbox in *MATLAB*

Then, the sampling time of data acquisition, which is 3E-5 seconds is input to the identification toolbox.

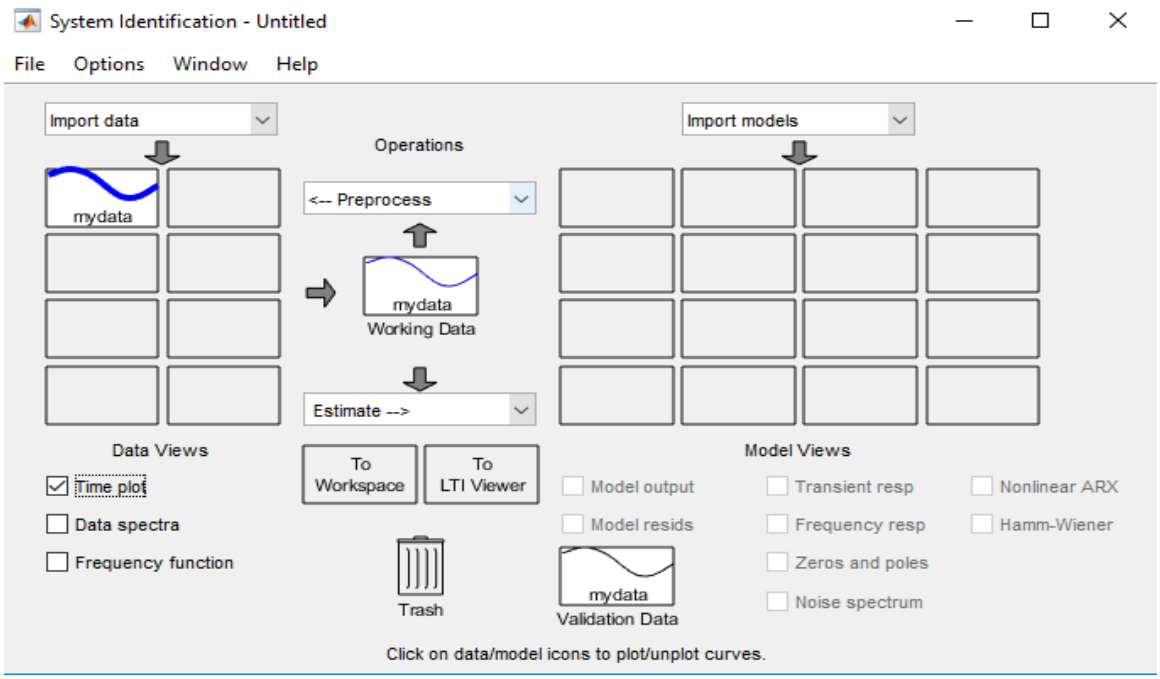

Figure 3.6: Data imported to the system identification toolbox in *MATLAB*

Now, the toolbox estimates and suggests the appropriate order for the transfer function of the piezo-cell system using the subspace approximation method as shown in Figure (3.7).

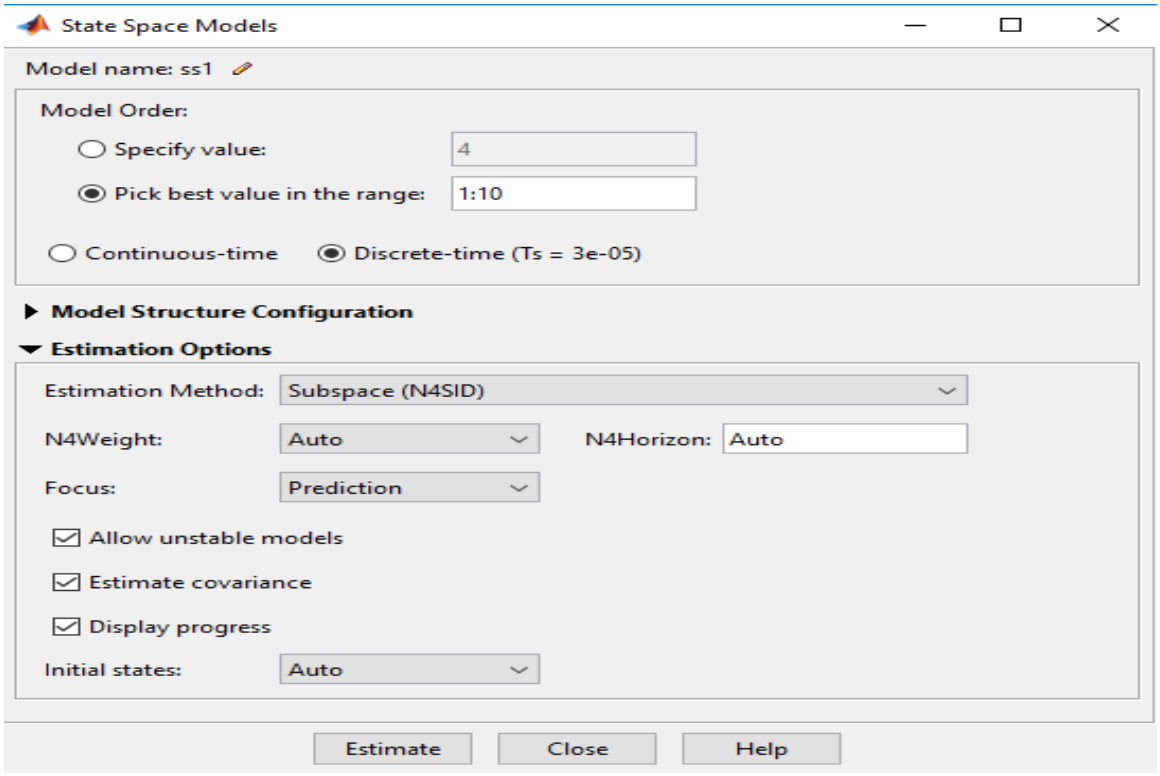

Figure 3.7: Using the subspace approximation method to find the optimal order of the system

The subspace approximation method basically uses the *'n4sid'* function in *MATLAB* to estimate the order. The input-output data (either in the time or the frequency domain), sampling time and the range of order of the system are the input arguments to the function. The optimal order for the system is selected from 1 to 10. It is suggested that a fifth order system is appropriate for the considered system.

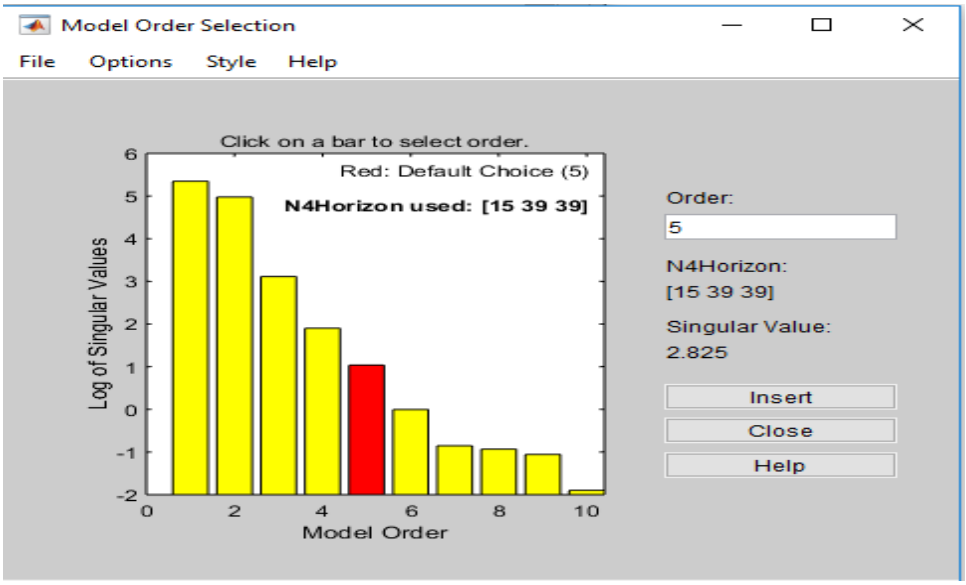

Figure 3.8: Identified model order of the system

So, the toolbox returns a discrete state-space model, which includes the matrices A, B, C, and D, representing the system, based on the input data, output data, the order and the sampling time supplied. Now, the continuous time model is determined from the discrete time model, by using the *d2cm* function in *MATLAB*, while employing the *Tustin* approximation method. The *'Tustin'* approximation method is generally used to achieve a good matching, in the frequency domain, between the discrete-time model and the continuous-time models. This method is also appropriate if our model has some crucial dynamics at any particular frequency. The *"Tustin"* approximation method, also known as the *"bilinear"* approximation method, also known as the "bilinear" approximation method, relating the z-domain and the s-domain transfer functions as follows :

$$z = e^{sT} \approx \frac{1 + sT/2}{1 - sT/2} \tag{3.1}$$

The discrete-to-continuous transformation is dependent on the following equation :

$$H(s) = H_d(z^{'}), \quad z^{'} = \frac{1 + sT/2}{1 - sT/2} \tag{3.2}$$

Thus, the continuous time state space model matrices AC, BC, CC and DC. Then, using the *"ss2tf"* function in $MATLAB$, the following continuous time transfer function of the system (sensor2/actuator1) is obtained :

$$TF = \frac{-2.85s^5 + 3.2E5s^4 - 8.24E9s^3 - 1.27E14s^2 + 6.27E18s - 7.46E21}{s^5 + 71439s^4 - 2.11E9s^3 + 1.12E13s^2 + 7.03E16s + 2.08E20} \tag{3.3}$$

Now, to verify the identification process output, the experiment is simulated in $ANSYS$ Workbench, by providing the same input impulse force data to the actuator 1. The output data (displacement of sensor 2) is obtained from the $ANSYS$ transient structural simulation as displayed in Figure (3.9).

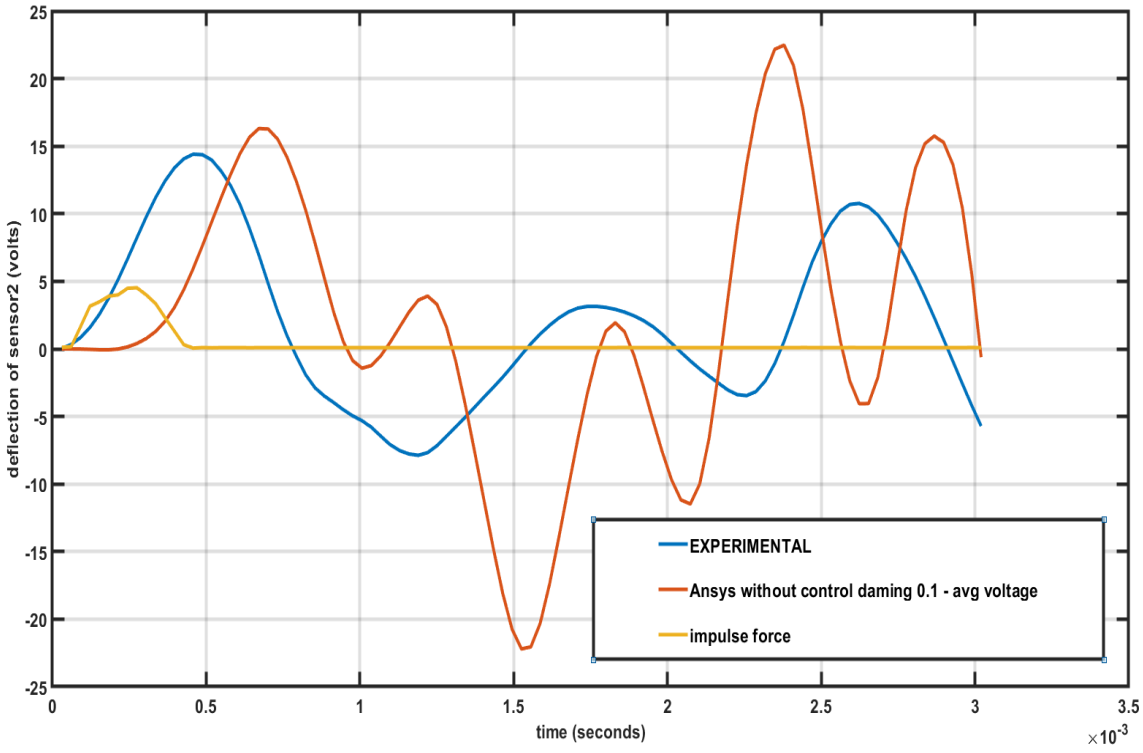

Figure 3.9: Displacement-time curve for the piezo-sensor 2 of the active acoustic metamaterial cell

3.3 Dynamic State-Space Feedback Control using *LabVIEW*

Now, once the system has been identified, a control system is implemented in order to control the propagation of acoustic waves through the medium. The schematic shown in Figure (3.10) displays the control system that needs to be implemented.

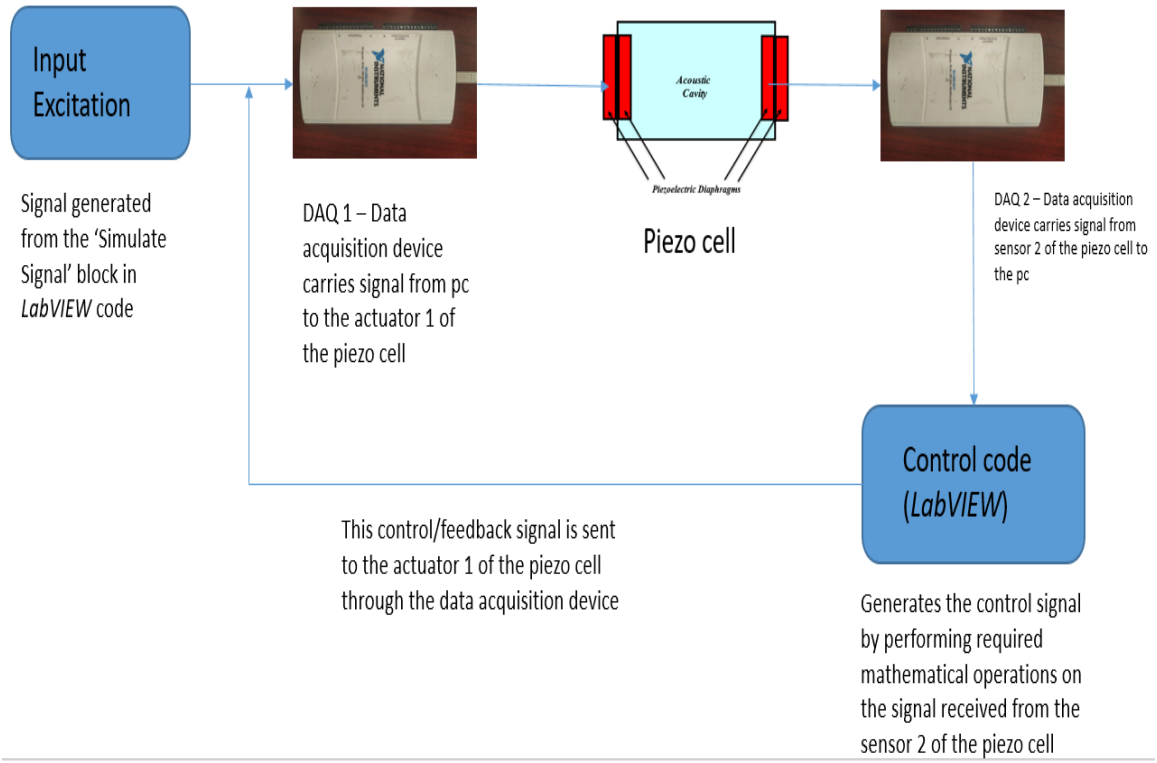

Figure 3.10: Dynamic control schematic diagram

A *LabVIEW* code along with the data acquisition device *NI-USB 6211* are employed to implement the controller. Using the *'simulate signal'* block in *LabVIEW*, an impulse is generated and sent to the piezo actuator 1 using the output pin of the *NI-USB 6211 DAQ* device. Using the *'DAQ Assistant'* module, the signal from the sensor 2 of the piezo cell is monitored, using the input pin of the *NI-USB 6211*. Then, the required mathematical operations are performed on this signal in order to generate the feedback signal. This feedback signal is sent to the actuator 1, which changes the effective input to the piezo cell and imparts control on the system. The *LabVIEW* code is displayed in the Figure (3.11).

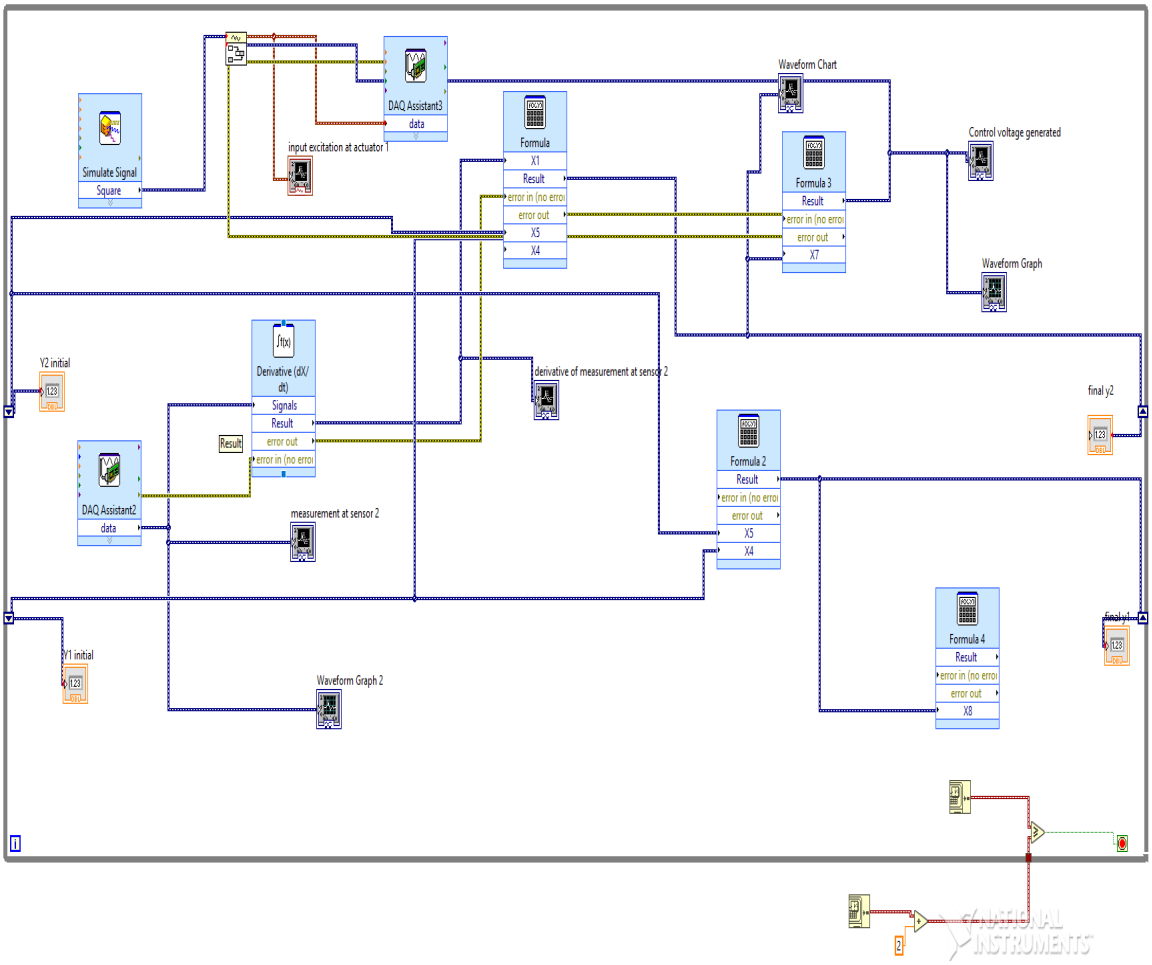

Figure 3.11: *LabVIEW* Code Block Diagram

The experiment is carried out for three different values of the gain : 0.0001, 0.00025 and 0.0005. Also, as seen in the schematic, 2 cases of different control gains are considered. In the first case, which is termed as the forward case or the normal case, the initial gain is set as $+K$ and second gain as $-K$. In the second case, which is termed as the reverse case, the initial gain is set as $-K$ and the second gain as $+K$. The results for both cases have been shown in Figures (3.12) through (3.19).

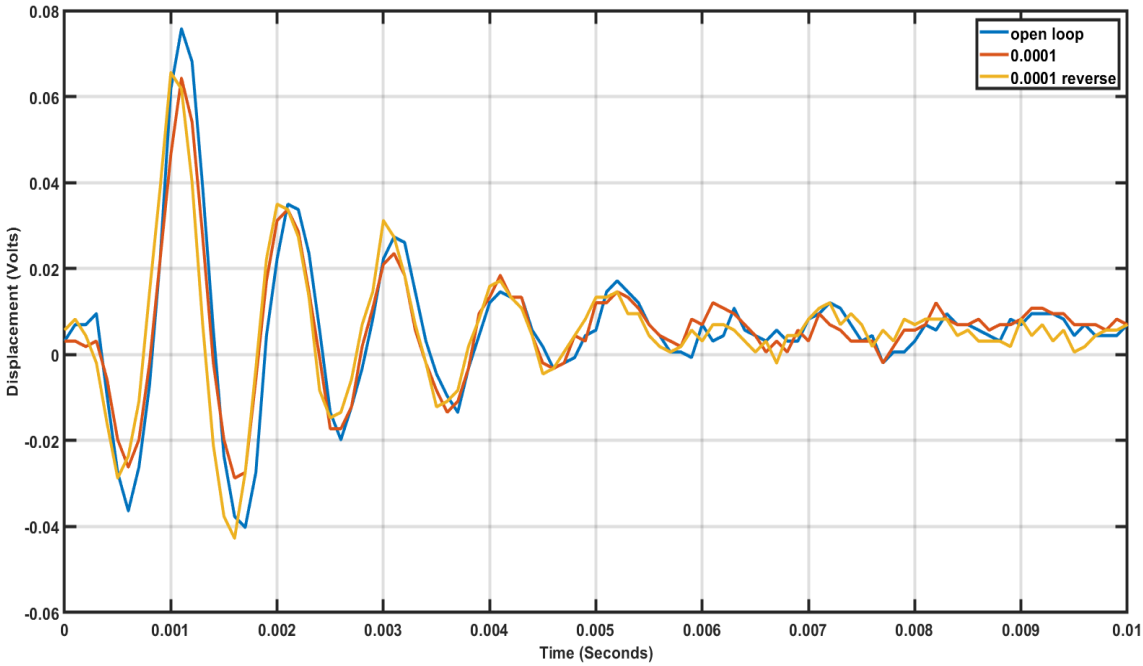

Figure 3.12: Displacement-time curve for the piezo-sensor 2 of the active acoustic metamaterial cell with gain 0.0001

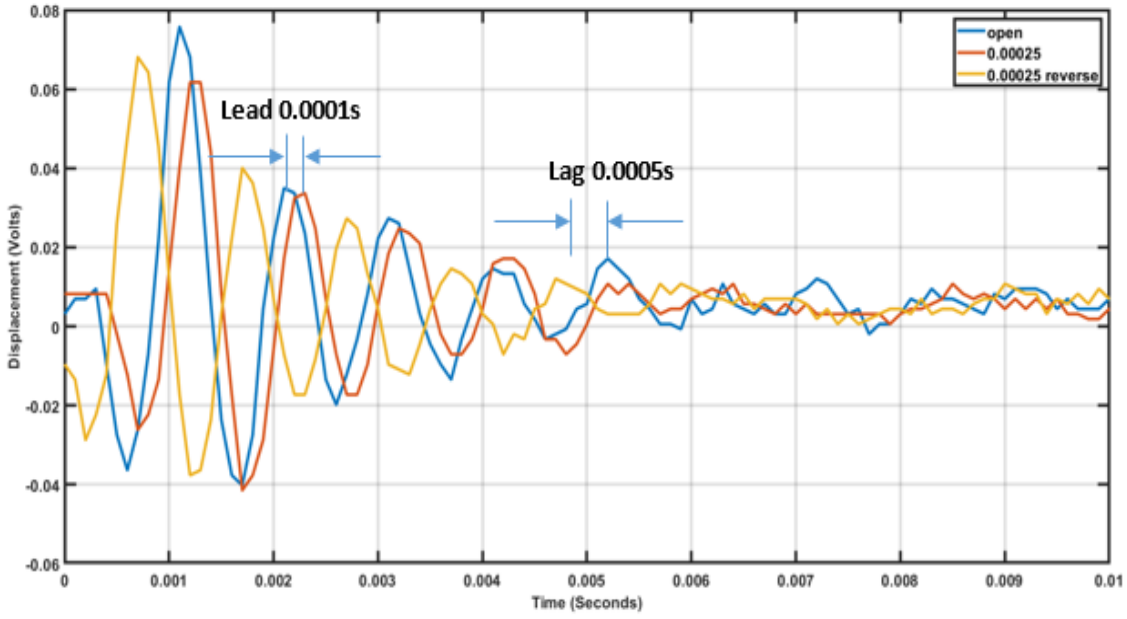

Figure 3.13: Displacement-time curve for the piezo-sensor 2 of the active acoustic metamaterial cell with gain 0.00025

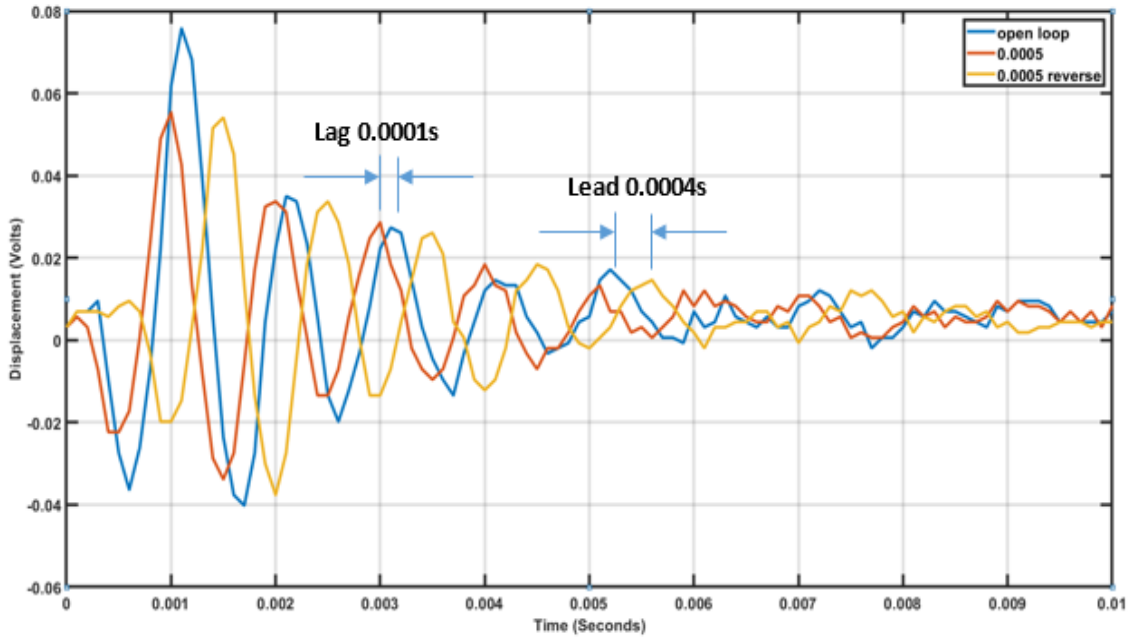

Figure 3.14: Displacement-time curve for the piezo-sensor 2 of the active acoustic metamaterial cell with gain 0.0005

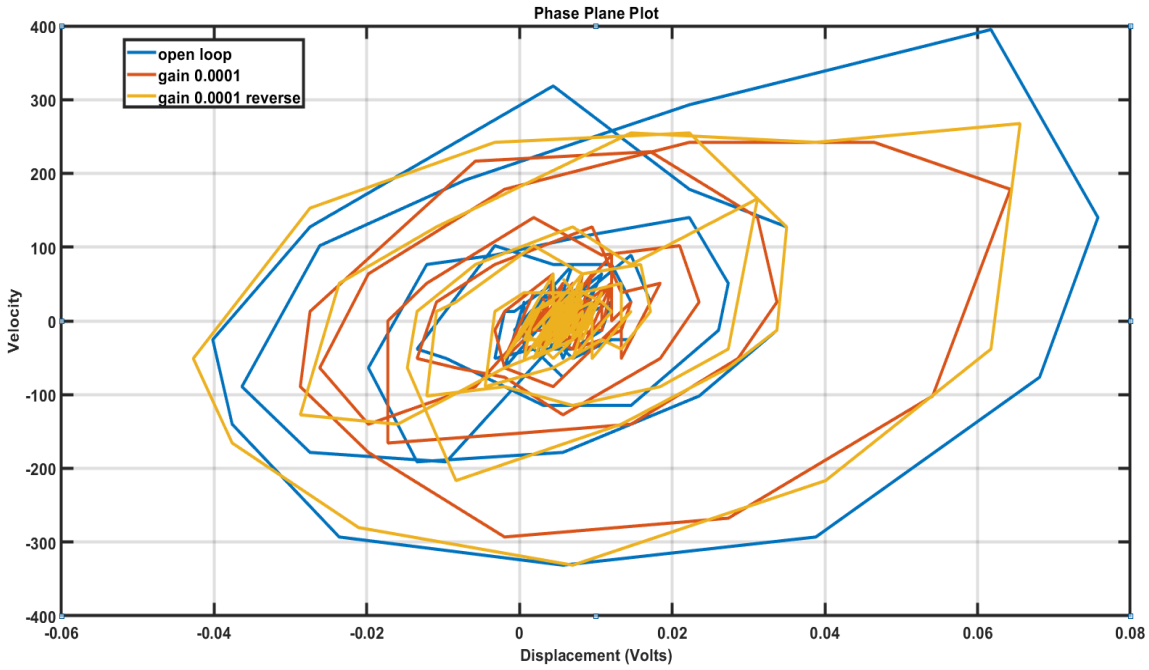

Figure 3.15: Phase plane plot for the piezo-sensor 2 of the active acoustic metamaterial cell with gain 0.0001

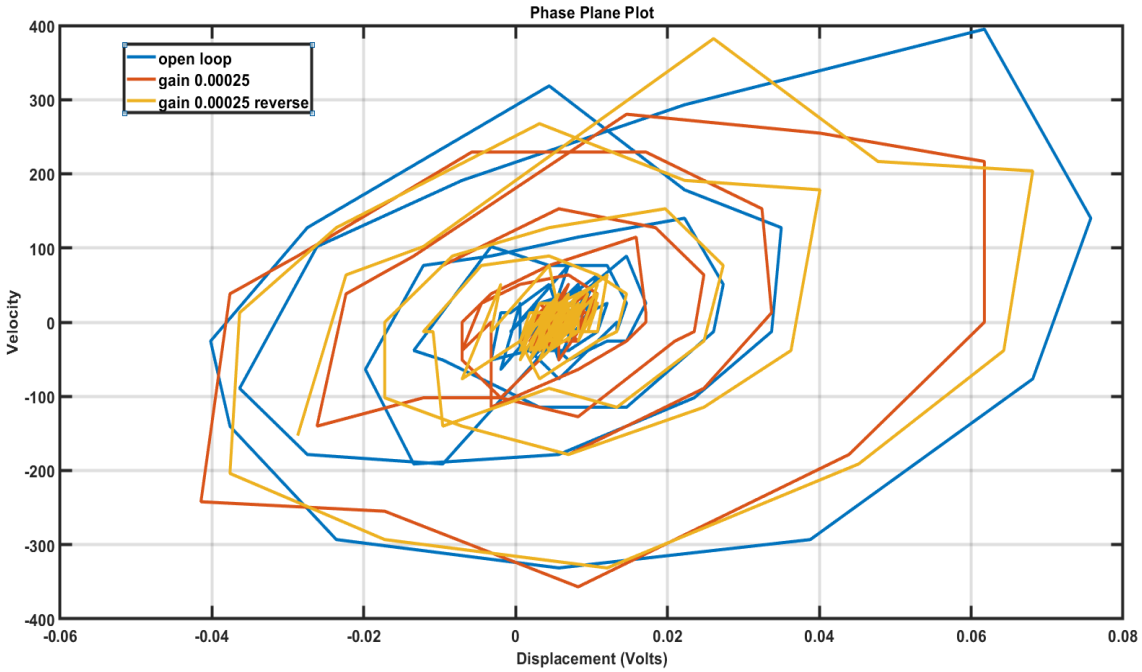

Figure 3.16: Phase plane plot for the piezo-sensor 2 of the active acoustic metamaterial cell with gain 0.00025

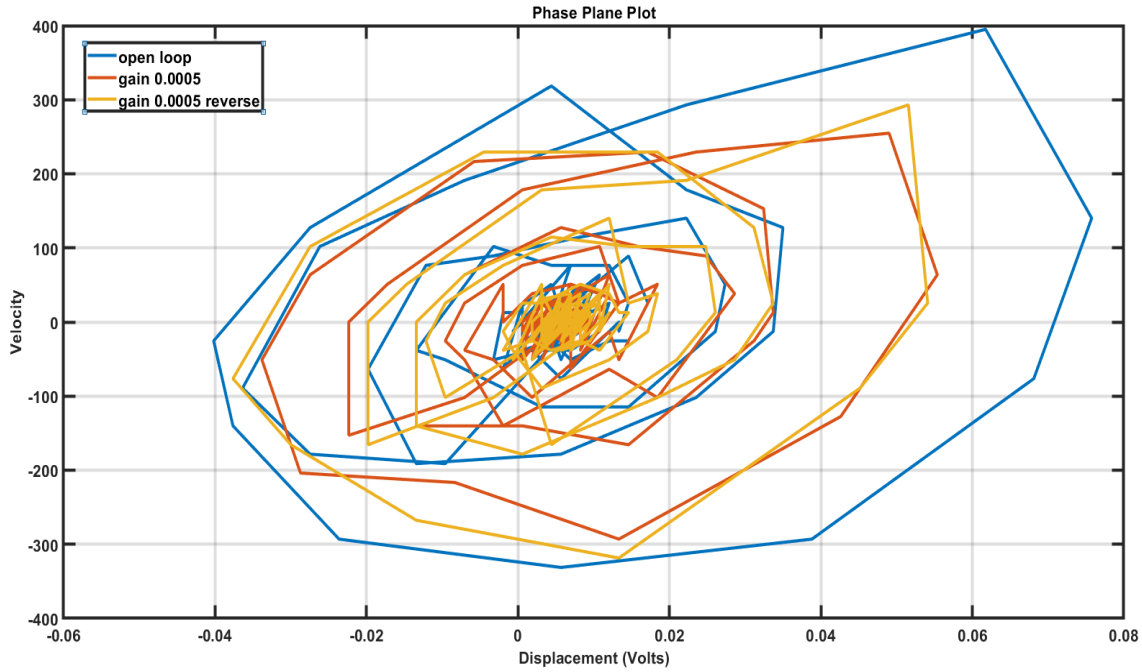

Figure 3.17: Phase plane plot for the piezo-sensor 2 of the active acoustic metamaterial cell with gain 0.0005

The above results show us the difference in the open-loop and closed-loop systems. The control forces which have been generated by the code, for impulse input, are shown below.

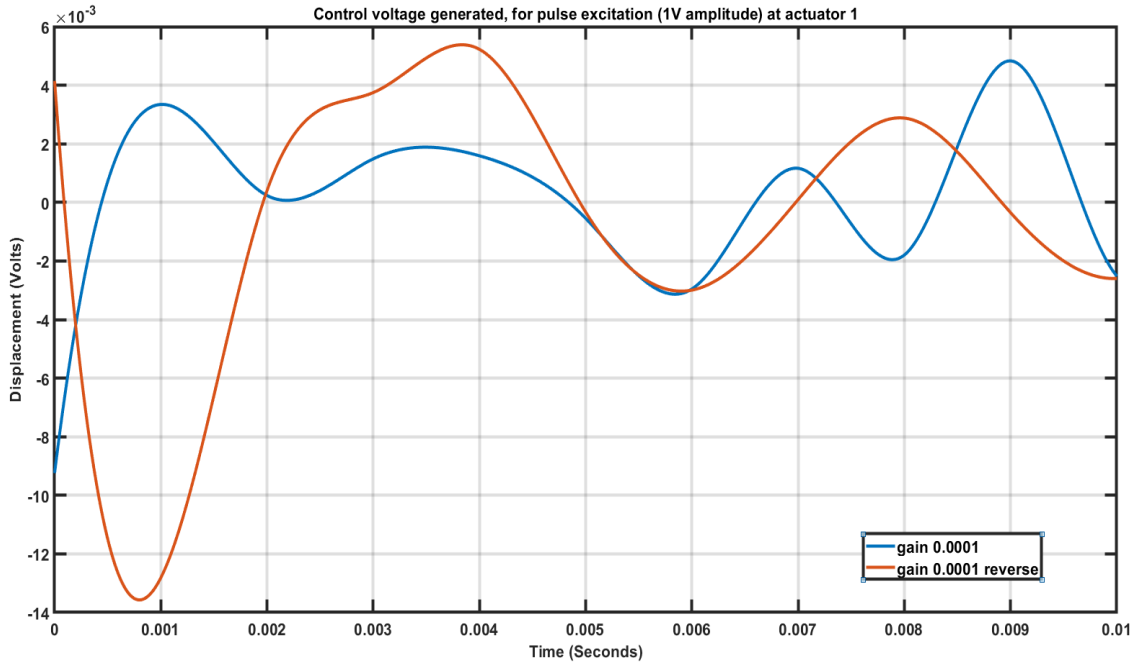

Figure 3.18: Control voltage-time curve for the control voltage generated with gain 0.0001

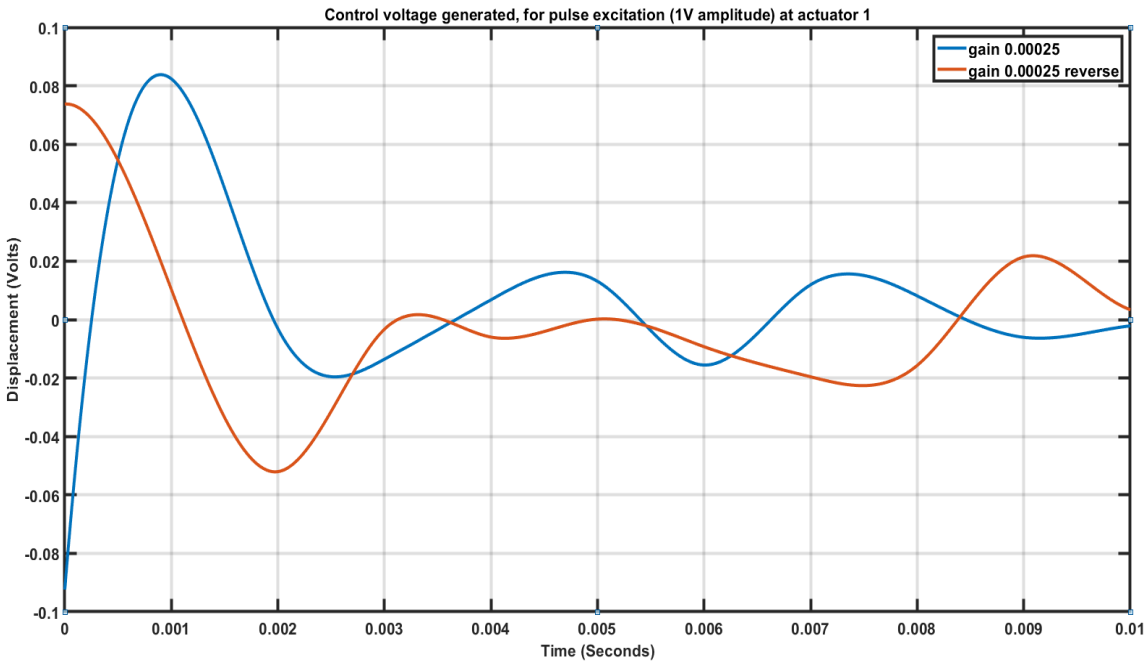

Figure 3.19: Control voltage-time curve for the control voltage generated with gain 0.00025

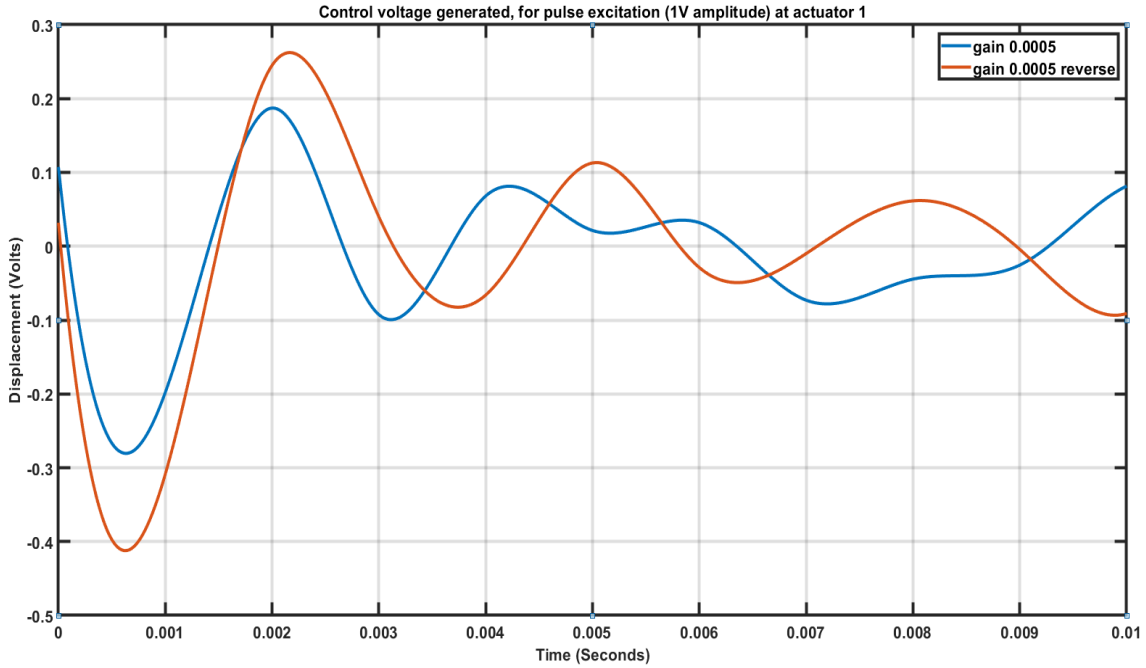

Figure 3.20: Control voltage-time curve for the control voltage generated with gain 0.0005

The lead and lag (due to phase difference) values for different cases of the three control gains are obtained as shown in Figure (3.21).

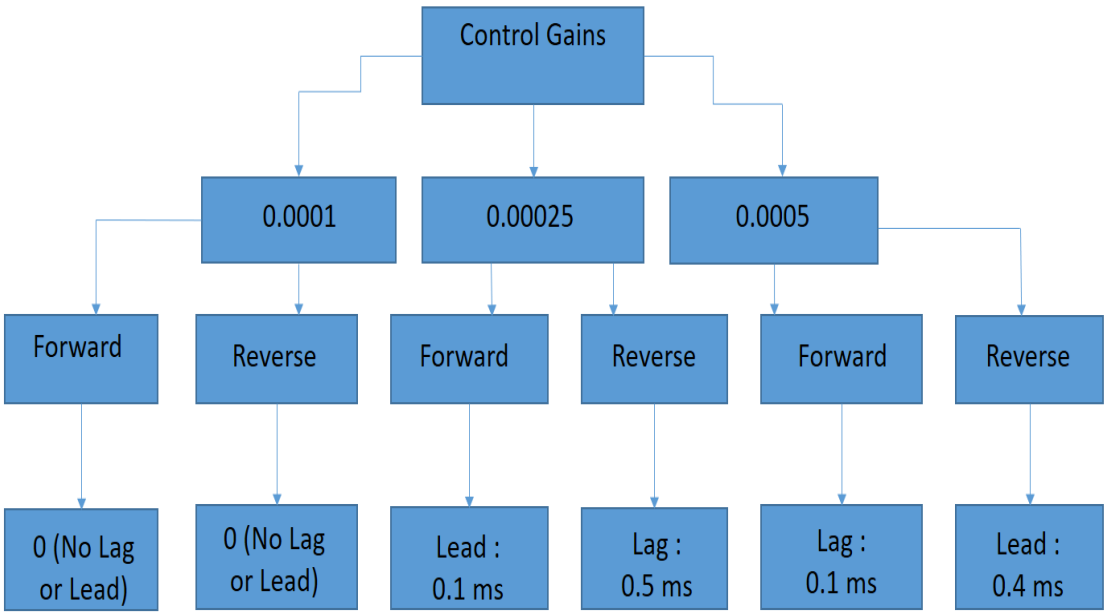

Figure 3.21: Phase difference for various gain values of control

Lead and lag as a function of various gain values is shown in Figures (3.22) and (3.23).

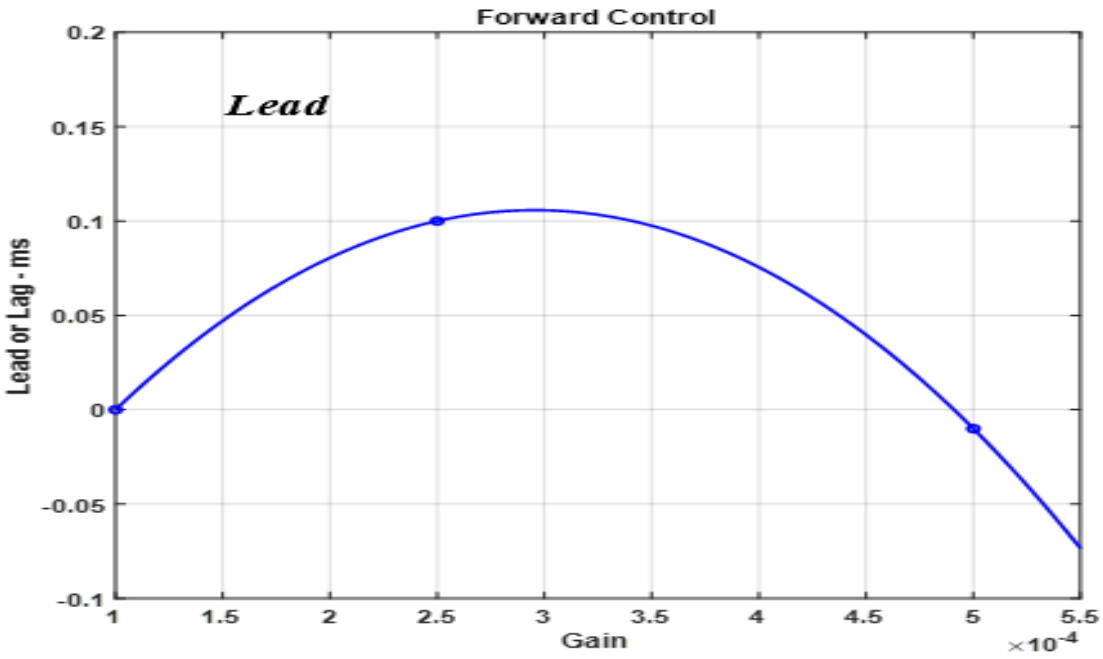

Figure 3.22: Phase difference for Forward Control

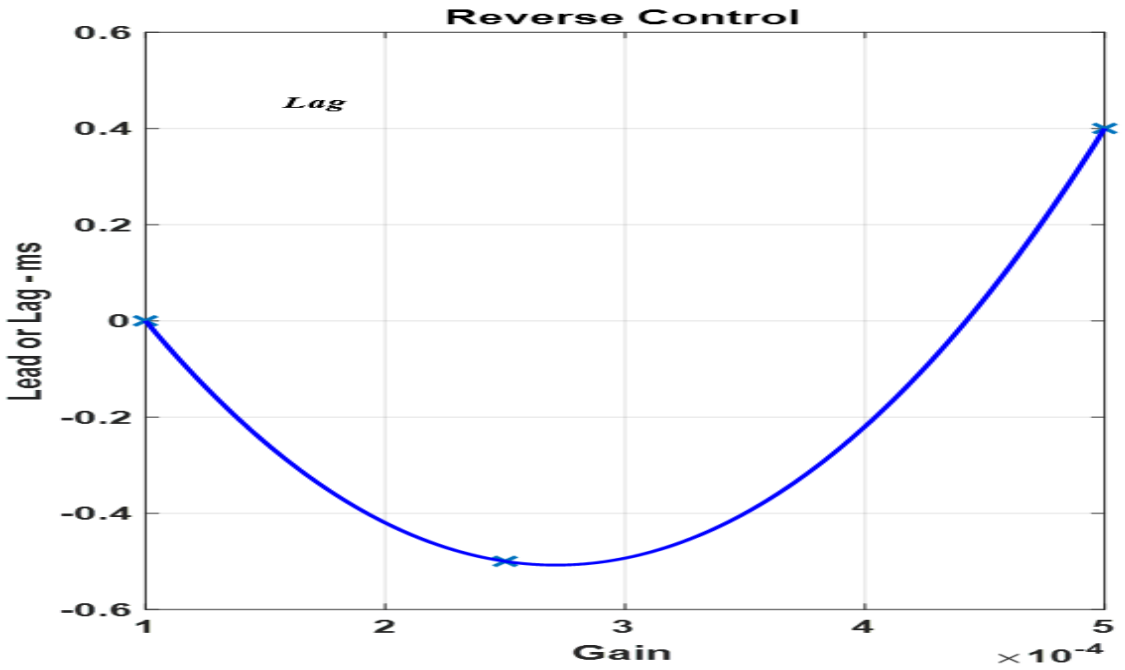

Figure 3.23: Phase difference for Reverse Control

3.4 Experimental Setup to measure Transmission Loss through the Active Acoustic Metamaterial Cell

Experiments are carried out to measure the transmission loss through the acoustic meta-cell. The experiments are carried out using the *ACUPRO TL* (transmission loss) tube to measure the *TL* of the cell as a function of frequency. The equipment consists of the main tube, the transmission loss tube, four microphones and a speaker, which are connected as shown in Figure (3.24). The two load method is adopted to obtain the transmission loss of the sample component. It is called the two load method, because the method requires two independent termination of the *TL* tube. These two terminations can be user-defined, where, the load A is a termination with open end and load B is a termination with closed end.

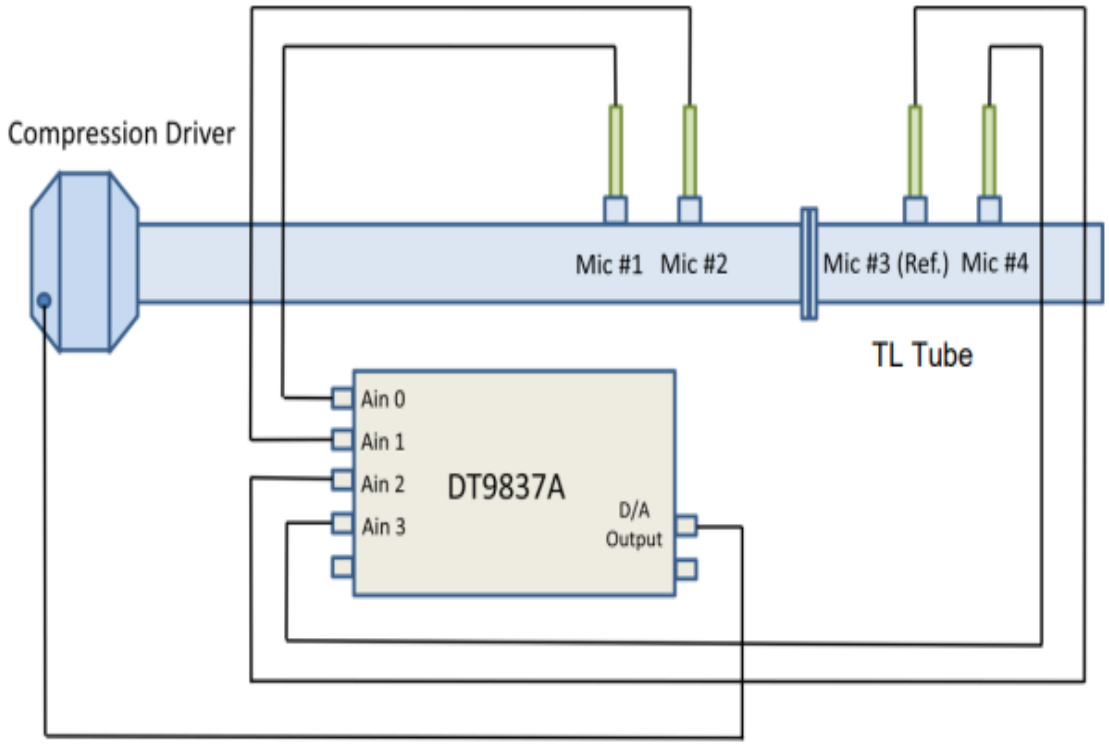

Figure 3.24: Experimental setup and connections for *TL* measurement

For the determination of accurate acoustical properties using the transmission loss tube, accurate phase measurements are required. The microphones should be in phase. Differences in phase of the microphones can cause error in the acoustical readings. Therefore, the standard phase calibration of the microphones, as mentioned in the manual, is a must.

The transmission tube is used for measuring the input-output data, calculating the transfer function and confirming the results of the transfer function data obtained from the impulse hammer test. The image of the setup is displayed in Figure (3.25).

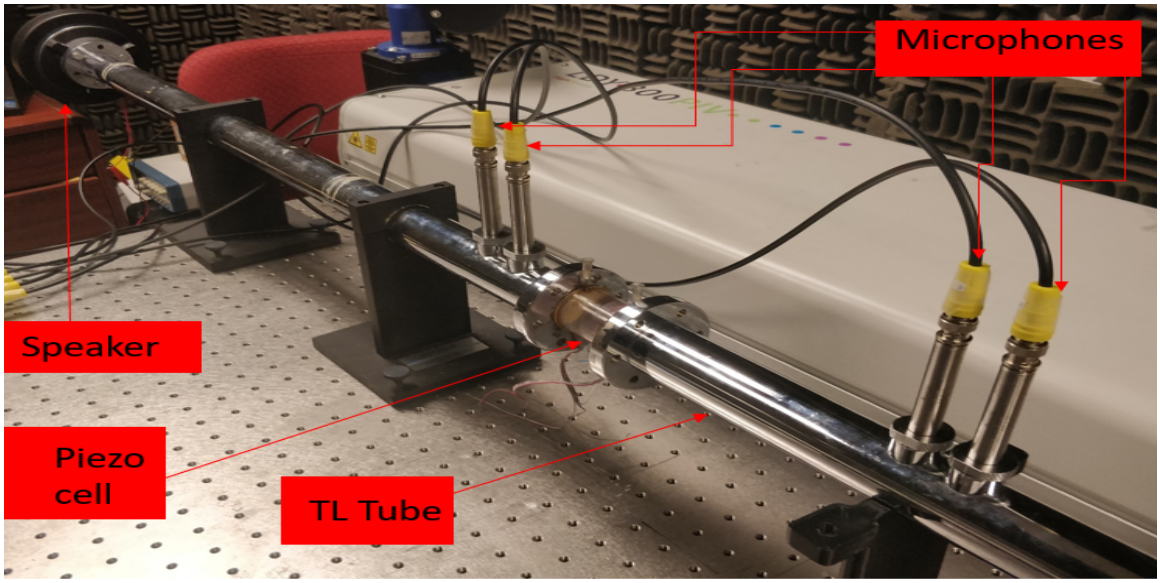

Figure 3.25: Transmission Loss tube experiment setup

The frequency response curve for the piezo cell obtained from the *TL* tube is shown in Figure (3.26).

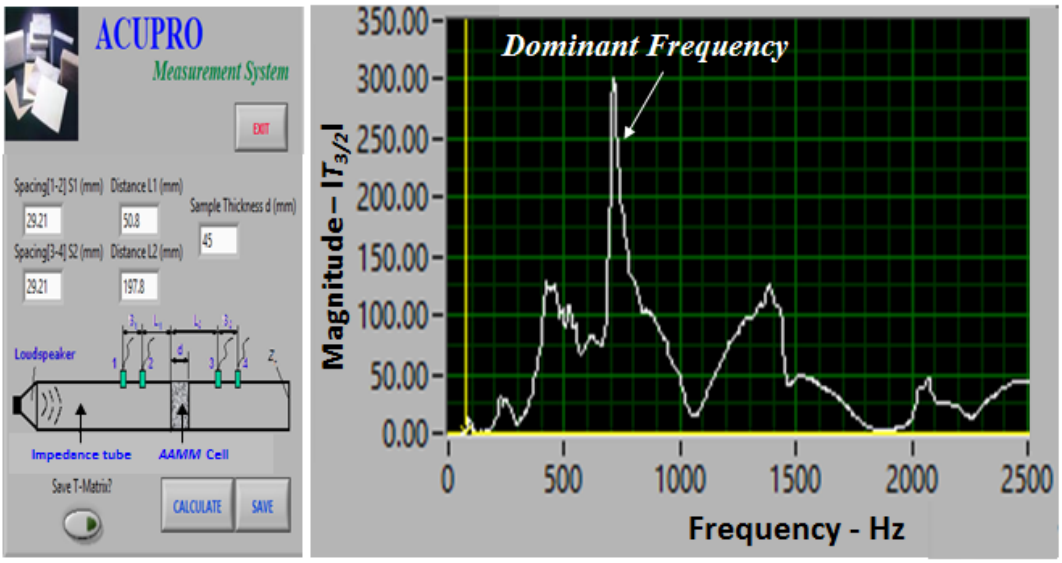

Figure 3.26: Results obtained from the Transmission Loss tube experiment setup

It can be seen from the curve that the dominant frequency of the system is

around 720 Hz, which is confirmed from the *ANSYS* simulation in the upcoming chapter. Thus, this experiment confirms the results obtained by the impulse hammer test.

3.5 Summary

This chapter describes the various experiments performed for system identification and active control of the piezo cell. The impulse hammer experiment (for system identification) has been described in detail. The post processing of data obtained from the experiment is being done in the system identification toolbox in *Matlab*. This chapter also describes and presents various results of the dynamic control of the system using *LabVIEW*. The results include the displacement-time plots, corresponding phase plane plots and the control voltages being generated from the control code, for three different values of the gain. At the end, the chapter describes the setup and the use of the *ACUPRO TL* (transmission loss) tube to carry out the verification of the system identification done by the impulse hammer method earlier.

Chapter 4: Finite Element Analysis

4.1 Overview

The first step in analyzing any given system in *ANSYS* is to create an accurate geometrical model of the system. The geometry was created using the Design Modeler module in *ANSYS*. The cylindrical cell has been bonded to brass and piezo films on both its ends.

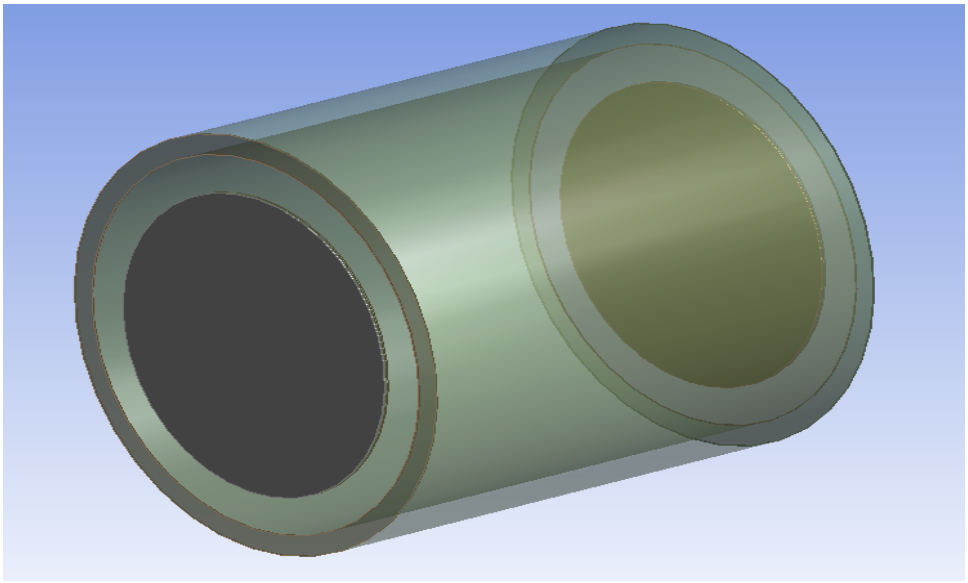

Figure 4.1: Geometrical model of the Active Acoustic Metamaterial Cell in the Design Modeler module in *ANSYS* Workbench

The next step in the analysis includes the input of engineering data from *ANSYS* library of various materials as well as from other material data bases. For the

piezo-cell model, three different materials are basically required. The cylindrical cell is made up of acrylic/plexiglass. The piezo *PZT4*, is considered as an orthotropic material, which includes the Youngs Modulus, Poissons Ratio and the Shear Modulus in the 3 axial directions. The properties of the Brass substrate is adopted from *ANSYS* engineering data.

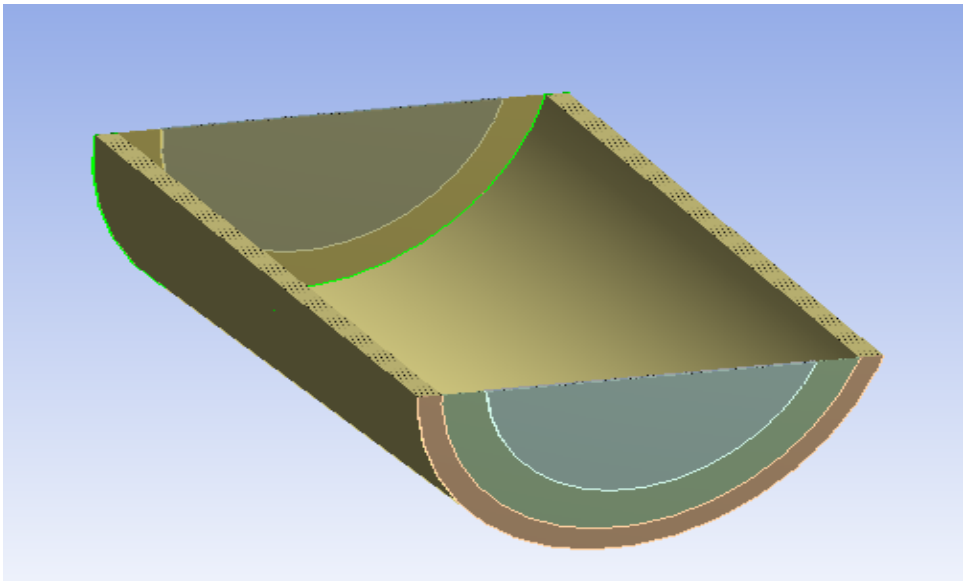

Figure 4.2: Cut-Section of the Active Acoustic Metamaterial Cell in *ANSYS* Workbench

The next step is to mesh the structure. Meshing divides the structure into a number of elements. The analysis basically analyzes the effect on each element, which in turn, gives us an idea about the behavior of the whole system (which is a combination of these elements). Since I have a 3D model, I have to use 3D elements to mesh the structure. Smaller element size generally gives more accurate results, but it is at a cost. The simulation-time increases exponentially with the increase in number of elements. I have used an element size of 1E-3 m. The size of each

element is 2E-3 m.

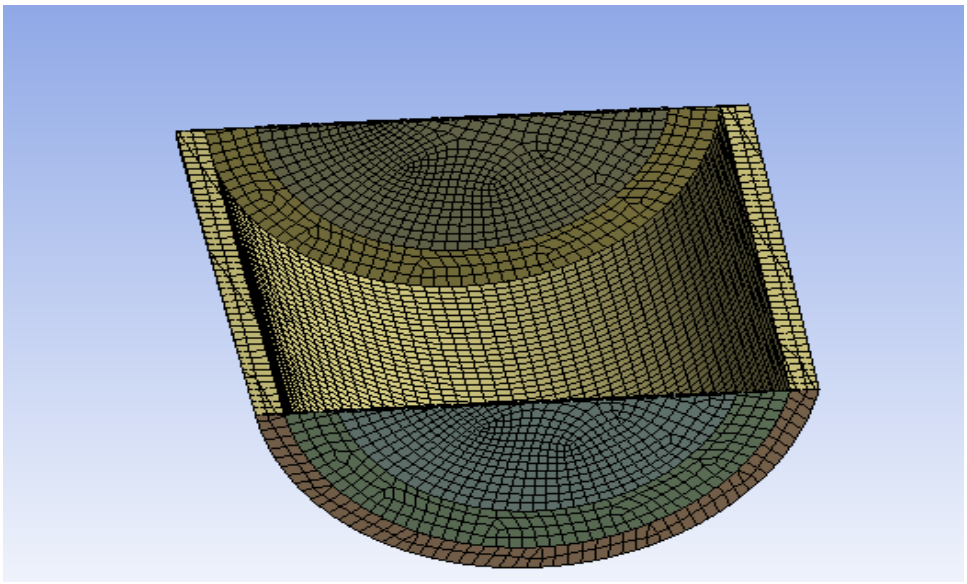

Figure 4.3: Meshed cut-section of the Active Acoustic Metamaterial Cell in *ANSYS* Workbench

After assigning the geometry and material properties as input to the system, different types of analysis are carried out on the system. These include Modal Analysis, Harmonic Analysis and Transient Structural Analysis.

4.2 Modal Analysis

Modal analysis allows users to find out the modes of any given system. It also simulates the systems mode shapes. It solves for the eigenvectors and the eigenvalues of the system. By simulating the system at different modes, we can identify which component is causing a certain mode and also, we can identify points which are likely to undergo large relative displacement, when vibrated at any given mode. First of all, we need to apply boundary conditions to any given system, before it can be

simulated. The translational degrees of freedom of the elements are constrained on the edge of the sides of the acrylic cylinder. The user can either select a frequency range or the maximum number of modes to find for the analysis. The modal analysis is carried out for 2 cases in particular. Firstly, the meta-cell is empty, and for the second case, it is filled with an acoustic fluid (water in this case). The results for case 1 have been shown in Figure (4.4).

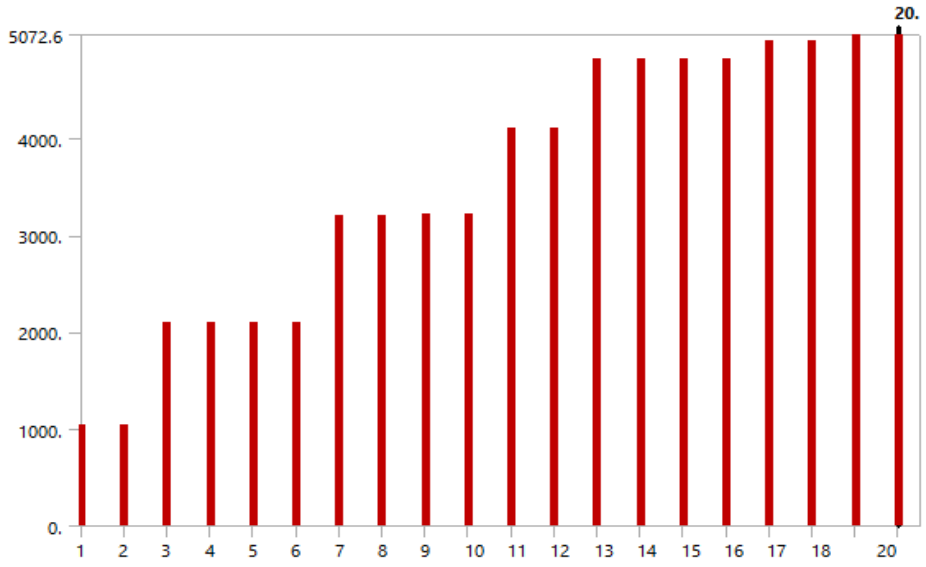

Figure 4.4: Modal Results from *ANSYS* Workbench for *AAMM* without any fluid inside the cavity

For the second case, the results have been shown in Figure(4.5).

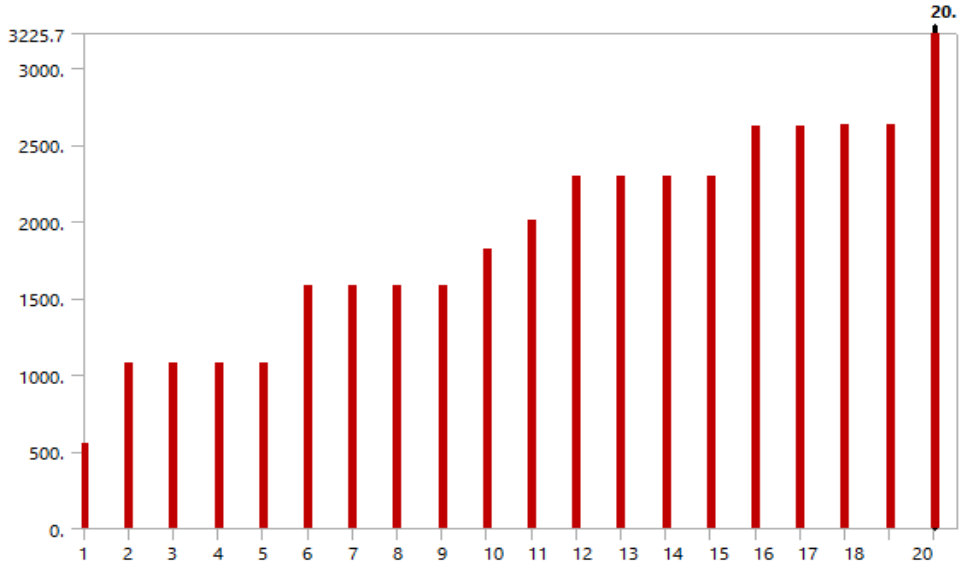

Figure 4.5: Modal results from *ANSYS* Workbench for *AAMM* Cell with water as the acoustic fluid inside the cavity

The modal analysis has been carried out for the first 20 modes of vibration. Figures (4.6) and (4.7) depict the first and second modes of vibration, which occur at the frequencies of 557 Hz and 1079 Hz respectively. These modes occur near the first two peaks obtained from the frequency response curve by the *TL* tube experiment, described in the previous chapter.

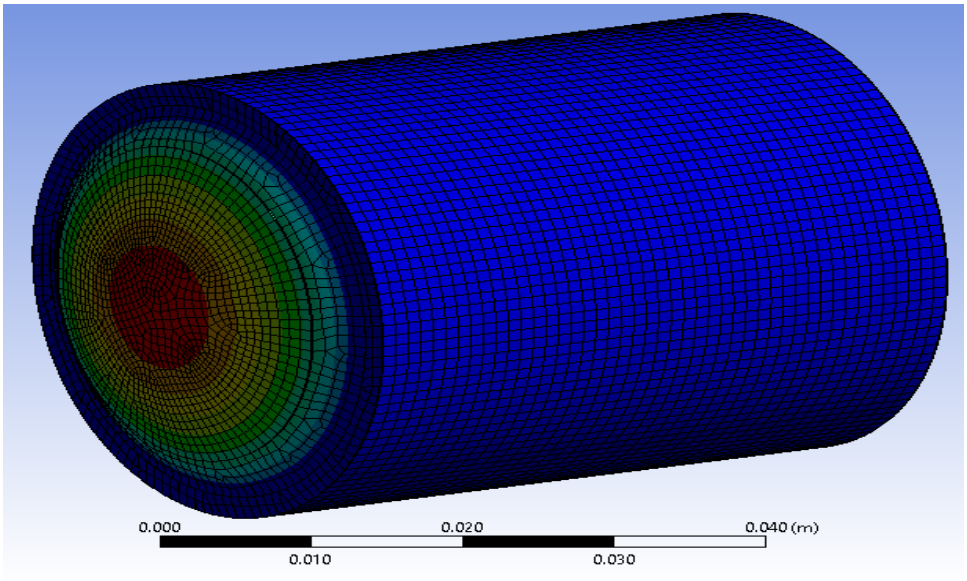

Figure 4.6: First mode of vibration of the *AAMM* Cell (557 Hz)

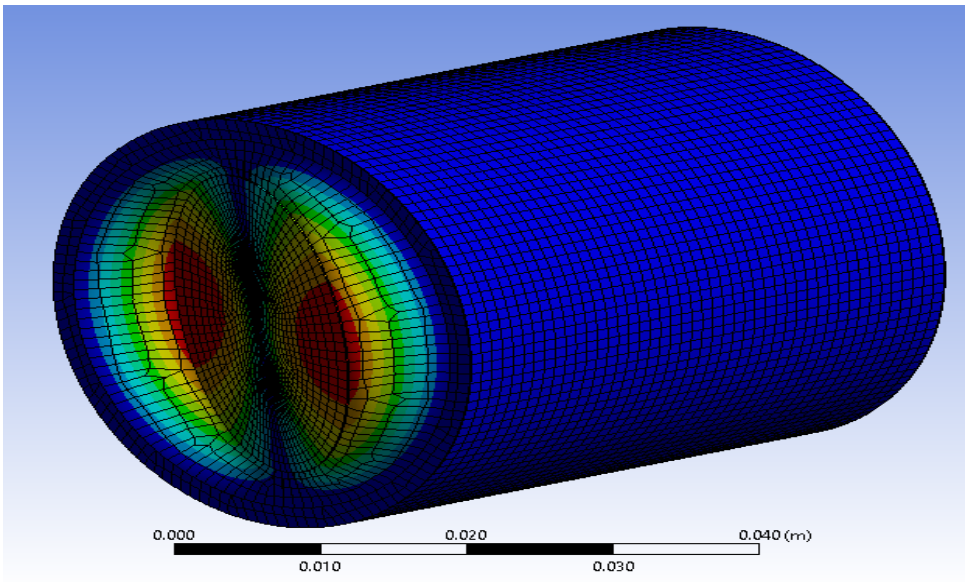

Figure 4.7: Second mode of vibration of the *AAMM* Cell (1079 Hz)

4.3 Harmonic Analysis

The harmonic analysis module in *ANSYS* workbench is used to perform harmonic analysis on the acoustic meta-cell. A harmonic response gives the frequency response at any given node, in the required direction. The analysis is used to obtain the harmonic response in the axial as well as radial direction of the cell.

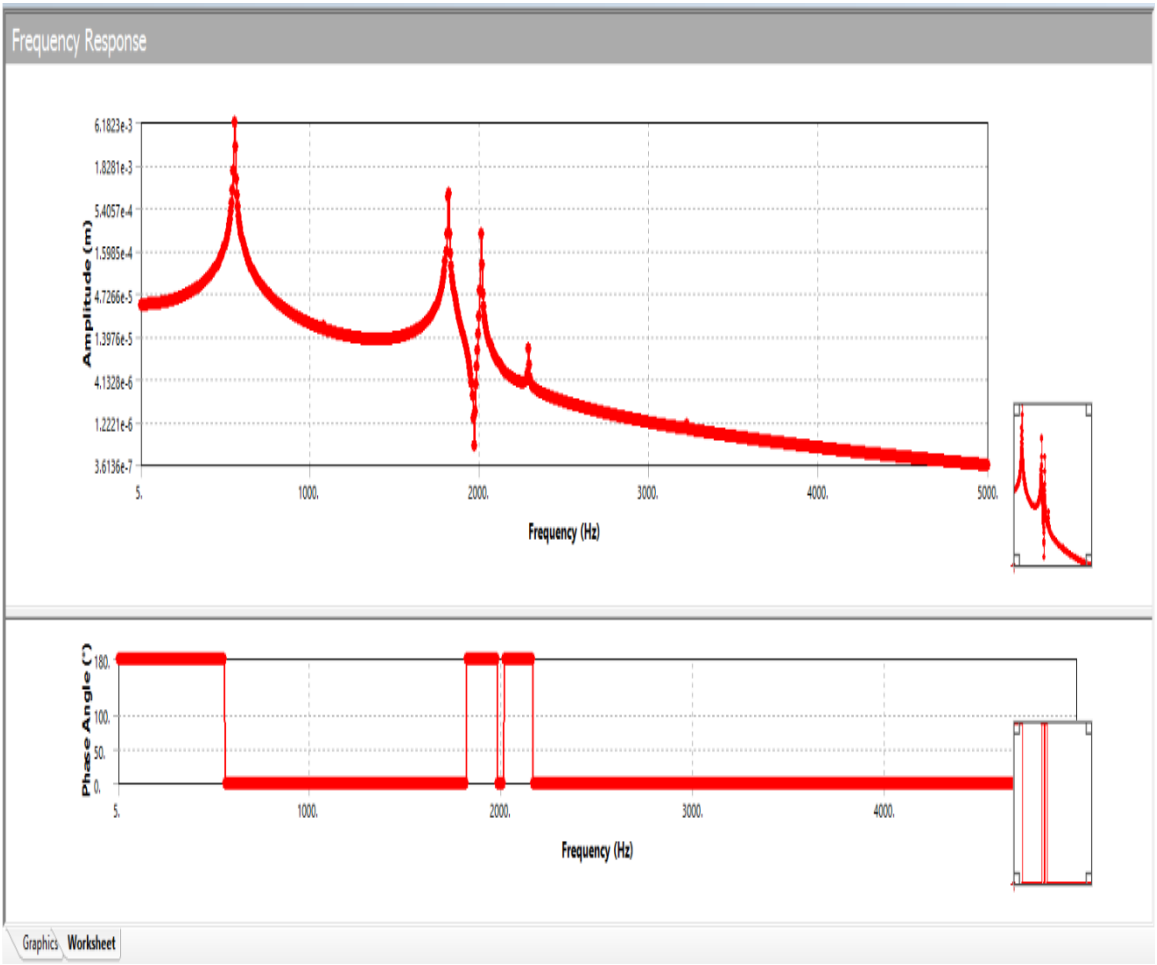

Figure 4.8: Frequency Response in the axial direction of the *AAMM* Cell

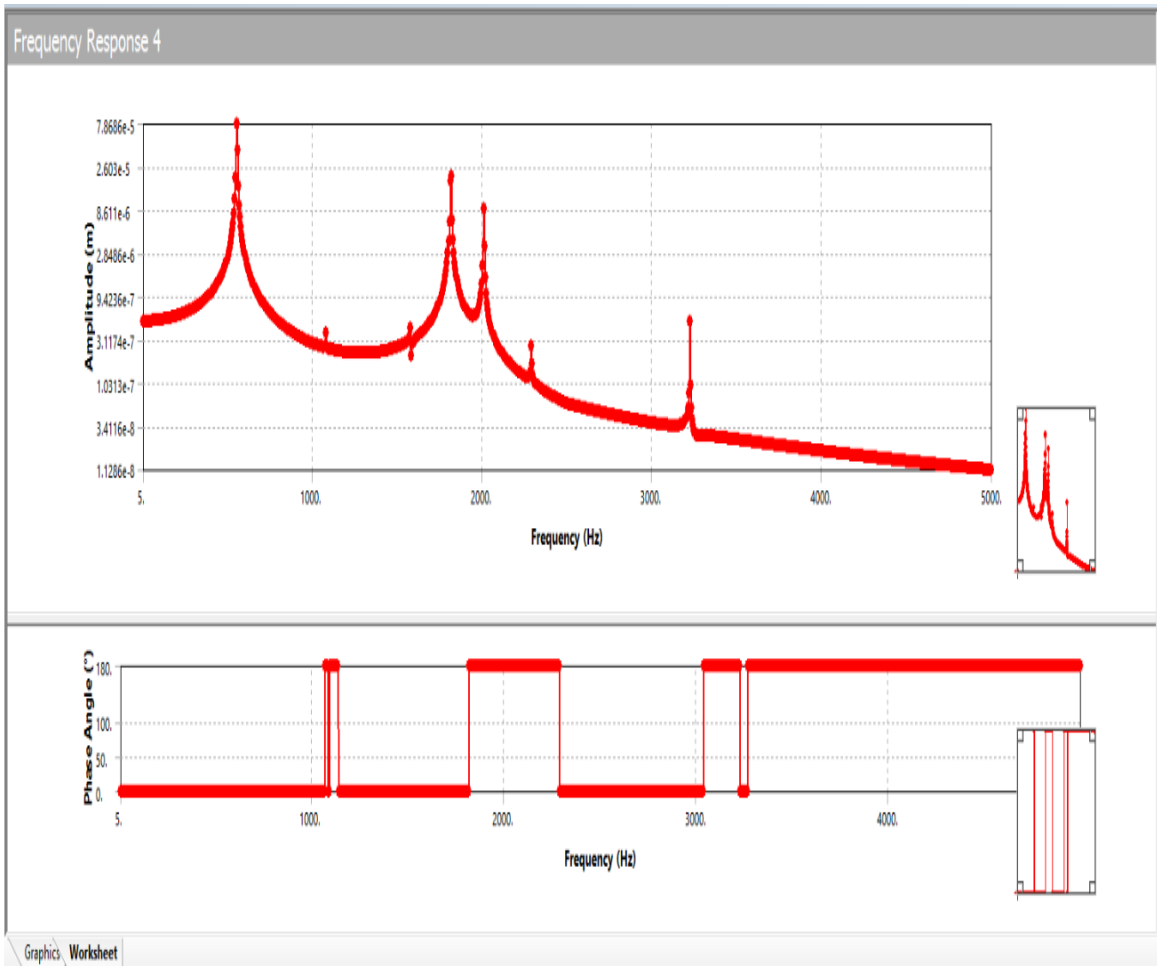

Figure 4.9: Frequency Response in the radial direction of the *AAMM* Cell

4.4 Transient Structural Analysis

The impulse hammer experiment is simulated in *ANSYS* using the transient structural module. The input force is an impulse to the piezo-actuator 1. The response of the piezo-sensor 2 is measured. The input force data has been collected from the impulse hammer experiment. The force being generated by the impulse hammer has been simulated as a time-based nodal force on a node on the piezo-actuator 1, as shown in Figure (4.8).

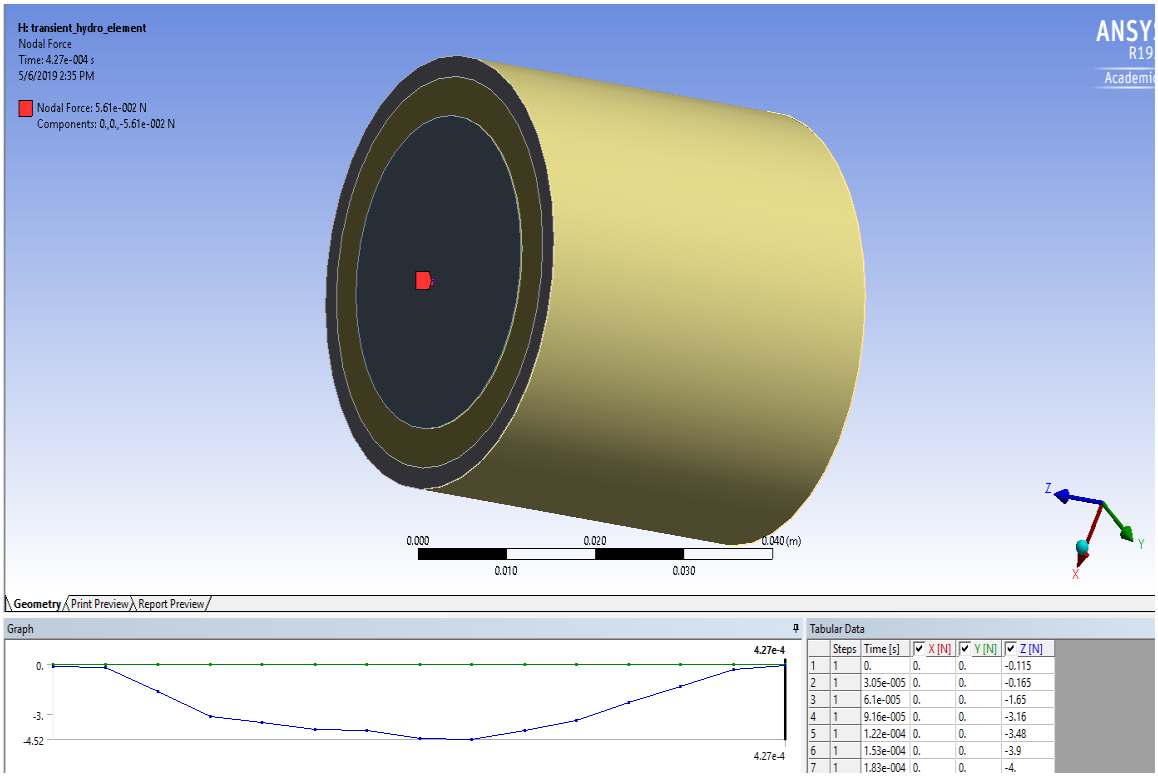

Figure 4.10: Application of impulse force on the Piezo-actuator 1 in *ANSYS* Workbench

The transient structural analysis has been run with a numerical damping coefficient of 0.1. The displacement caused on piezo-sensor2 due to the impulse force on piezo-actuator 1, generates voltage on the piezo-sensor2. The variation of this voltage as well as displacement are plotted with respect to time. Also, a dynamic state-space feedback control is implemented on the model, using *APDL* commands in *ANSYS* Workbench.

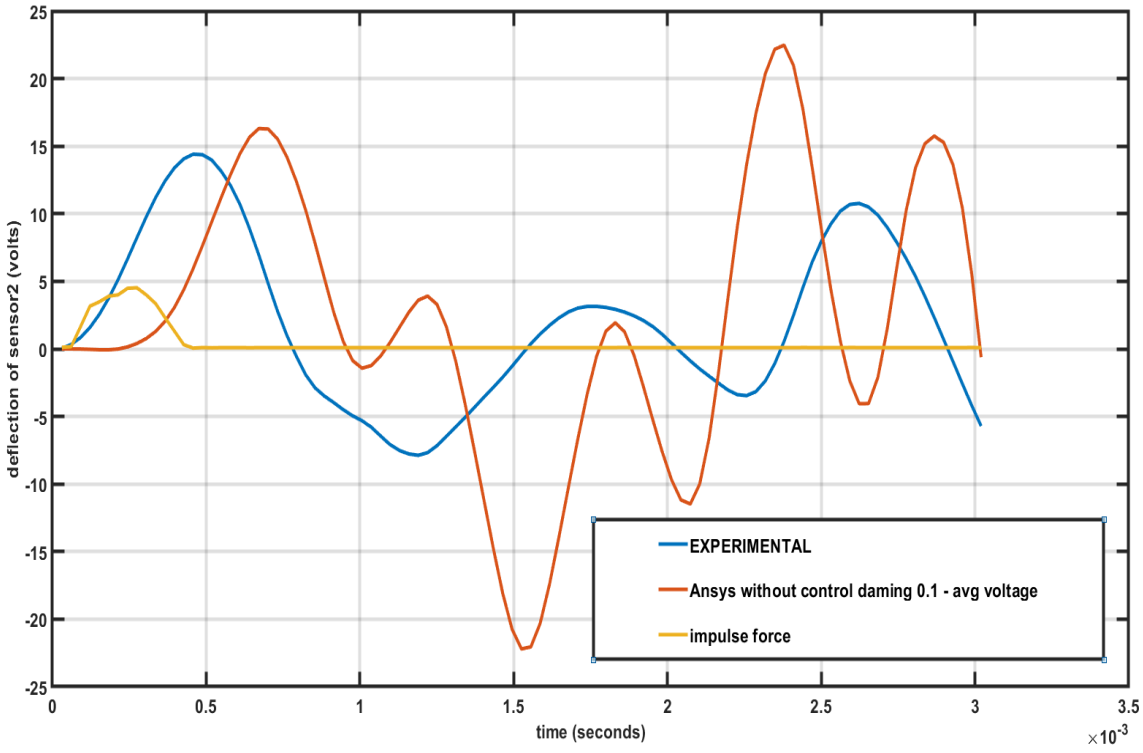

Figure 4.11: Comparison of *ANSYS* Workbench results with the experimental results

4.5 Summary

This chapter describes the Finite Element Analysis *(FEA)* simulation being carried out in order to validate the experimental results. The chapter starts by describing the geometrical properties of the piezo cell and the process of meshing it in *ANSYS* Workbench. Three types of analysis have been described : Modal, harmonic and the transient structural analysis. The transient structural analysis simulates the impulse hammer experiment, described in the previous chapter. The displacement-time plot comparing the experimental and the simulation results has been presented.

Chapter 5: Conclusions and Recommendations

5.1 Conclusions

This thesis has presented a comprehensive theoretical and experimental investigations of a new class of active nonreciprocal metamaterials *(ANAM)*. The proposed *ANAM* relies in its operation on acoustic cavities with controlled piezoelectric boundaries. These boundaries are controlled with novel dynamic controller that generates a gyroscopic coupling between the controller and the meta-cell to generate the necessary non-reciprocal behavior.

The theory of the dynamic controller are presented in great details to demonstrate the effectiveness of the generated gyroscopic coupling in developing and enhancing the non-reciprocal behavior of the cell. The stability of the controller is investigated and proofed using Lyapunov stability criterion.

The *ANAM*-cell with the controller are modeled using the commercial finite element package *ANSYS*. The theoretical performance characteristics of the system are predicted by *ANSYS*. Experimental validation of the theoretical predictions is determined using a prototype of the meta-cell. The dynamics of the cell are identified using impulse response of the cell. The identified model is checked against the theoretical predictions of *ANSYS*. Then, the non-reciprocal experimental behavior

of the meta-cell is demonstrated through extensive testing using various control gains. The obtained results show clearly the effectiveness of the dynamic controller in generating the non-reciprocal behavior of the meta-cell.

5.2 Recommendations for Future Studies

Although the present work has addressed the problem of non-reciprocal acoustic behavior of metamaterial by using novel dynamic control action, many issues remain to be considered in future studies. Important among these issues is to extend this work to multi-cell configurations where coupling will not only be between the cell and controller but also between neighboring cells.

Also, comparisons are needed to establish the limitations and merits of the dynamic controller as compared to other techniques of generating non-reciprocal behavior such as temporal and spatial modulation method *(TSMM)*. The application of the *TSMM* can be readily applied to the current meta-cell configuration and the relative merits of the two techniques can be established.

Further work is needed to study the impedance and reflectivity characteristics of the *ANAM* cell both theoretically and experimentally in order to develop a complete picture of the acoustical behavior of the cell.

A natural extension of this work is to develop maps of the acoustical energy flow across a unit cell and multi-cell configurations both in the forward and backward directions with and without the dynamic controller as well as with the conventional *TSMM* approach.

Bibliography

[1] P. Samarasinghe and T. D. Abhayapala, "Acoustic reciprocity : An extension to spherical harmonics domain", *The Journal of the Acoustical Society of America*, Vol. 142, EL337, 2017.

[2] C. P. A. Wapenaar, M. W. P. Dillen and J. T. Fokkema, "Reciprocity theorems for electromagnetic or acoustic one-way wave fields in dissipative inhomogeneous media", *Radio Science*, Vol. 36, No. 5, pp. 851-863, 2001.

[3] J. -S. Chen, I-L. Chang, W. -T. Huang, L. -W. Chen and G. -H. Huang, "Asymmetric transmission of acoustic waves in a layer thickness distribution gradient structure using metamaterials", *AIP Advances*, Vol. 6, pp. 095020, 2016.

[4] E. Walker, A. Neogi, A. Bozhko, Yu. Zubov, J. Arriaga, H. Heo, J. Ju, and A. A. Krokhin, "Nonreciprocal linear transmission of sound in a Viscous Environment with Broken P Symmetry", *Physical Review Letters*, Vol. 120, pp. 204501, 2018.

[5] D. -D. and X. -F. Zhu, "An effective gauge potential for nonreciprocal acoustics", *EPL (Europhysics Letters)*, Vol. 102, No. 1, 2013.

[6] D. Beli, P. B. Silva, J. R. de Frana Arruda, "Mechanical circulator for elastic waves by using the nonreciprocity of flexible rotating rings", *Mechanical Systems and Signal Processing*, Vol. 98, pp. 1077-1096, 2018.

[7] S. Karkar and M. Collet, "Nonreciprocal acoustics using programmable boundary conditions : from boundary control and active metamaterials to the acoustic diode", *SMASIS*, 2017.

[8] M. Naghdi and F. Farzbod, "Acoustic nonreciprocity in Coriolis mean flow systems", *The Journal of the Acoustical Society of America*, Vol. 143 230, 2018.

[9] A. Baz, "The structure of an active acoustic metamaterial with tunable effective density", *New Journal of Physics*, Vol. 11, pp. 123010 (16pp), 2009.

[10] A. Baz, "Active nonreciprocal acoustic metamaterials using a switching controller", *The Journal of the Acoustical Society of America*, Vol. 143, pp. 1376, 2018.

[11] H. Ramezani, M. Dubois, Y. Wang, Y R. Shen, and X. Zhang, "Directional excitation without breaking reciprocity", *Physical Review Applied*, Vol. 9 034033, 2018.

[12] A. Merkel, M. Willatzen, and J. Christensen, "Dynamic Nonreciprocity in Loss-Compensated Piezophononic Media", *New J. Phys.*, Vol. 18 095001, 2016.

[13] L. Ranzani and J. Aumentado, "A geometric description of nonreciprocity in coupled two-mode systems", *New Journal of Physics*, Vol. 16 103027, 2014.

[14] A. Ishikawa and K. Tsuruta, "Design of Non-Reciprocal Acoustic Waveguides by Indirect Interband Transitions", *Proceedings of Symposium on Ultrasonic Electronics*, Vol. 37, 2016.

[15] H. Nassar, H. Chen, A. N. Norris, M. R. Haberman and G. L. Huang, "Nonreciprocal wave propagation in modulated elastic metamaterials", *Proc. R. Soc. A*, Vol. 473: pp. 20170188, 2017.

[16] M.A. Attarzadeh, H. Al Ba'ba'a, M. Nouh, "On the wave dispersion and nonreciprocal power flow in space-time traveling acoustic metamaterials", *Applied Acoustics*, Vol. 133, pp. 210-214, 2018.

[17] Y. Wang, B. Yousefzadeh, H. Chen, H. Nassar, G. Huang and C. Daraio, "Observation of Nonreciprocal Wave Propagation in a Dynamic Phononic Lattice", *Physical Review Letters*, Vol. 121, 194301, 2018.

[18] B. -I. Popa and S. A. Cummer, "Non-reciprocal and highly nonlinear active acoustic metamaterials", *Nature Communications*, Vol. 5, Article number: 3398, 2014.

[19] K. J. Moore, J. Bunyan, S. Tawfick, O. V. Gendelman, S. Li, M. Leamy and A. F. Vakakis, "Nonreciprocity in the dynamics of coupled oscillators with nonlinearity, asymmetry, and scale hierarchy", *Physical Review E*, Vol. 97, 012219, 2018.

[20] N. Alujevi, I. Senjanovi, I. atipovi and N. Vladimir, "The absence of reciprocity in active structures using direct velocity feedback", *Journal of Sound and Vibration*, Vol. 438, pp. 251-256, 2019.